
Article:
Ausiannikava, Darya, Mitchell, Laura, Marriott, Hannah et al. (6 more authors) (2018) Evolution of Genome Architecture in Archaea : Spontaneous Generation of a New Chromosome in Haloferax volcanii. Molecular Biology and Evolution. pp. 1855-1868. ISSN 0737-4038

https://doi.org/10.1093/molbev/msy075

Article – Discoveries

Evolution of Genome Architecture in Archaea: Spontaneous Generation of a New Chromosome in *Haloferax volcanii*

Darya Ausiannikava[a#], Laura Mitchell[a], Hannah Marriott[a], Victoria Smith[a], Michelle Hawkins[a†], Kira S. Makarova[b], Eugene V. Koonin[b], Conrad A. Nieduszynski[c], Thorsten Allers[a*]

School of Life Sciences, University of Nottingham, Queen's Medical Centre, Nottingham, UK[a]; National Center for Biotechnology Information, National Library of Medicine, NIH, Bethesda, Maryland, USA[b]; Sir William Dunn School of Pathology, University of Oxford, South Parks Road, Oxford OX1 3RE, UK[c]

Short title: Evolution of genome architecture in Archaea

***Correspondence:** thorsten.allers@nottingham.ac.uk Tel. +44 115 823 0304

#Current address: School of Biological Sciences, Institute of Cell Biology, University of Edinburgh, Kings Buildings, Edinburgh EH9 3FF, UK

†Current address: Department of Biology, University of York, Wentworth Way, York YO10 5DD, UK

Keywords: Chromosome; Genome architecture; Multipartite genome; Homologous recombination; Genome stability; Archaea; *Haloferax volcanii*

Word count (Abstract): 150

Word count (Text, excluding abstract, methods, figure legends, and references): 4,978

Abstract

The common ancestry of archaea and eukaryotes is evident in their genome architecture. All eukaryotic and several archaeal genomes consist of multiple chromosomes, each replicated from multiple origins. Three scenarios have been proposed for the evolution of this genome architecture: (1) mutational diversification of a multi-copy chromosome; (2) capture of a new chromosome by horizontal transfer; (3) acquisition of new origins and splitting into two replication-competent chromosomes. We report an example of the third scenario: the multi-origin chromosome of the archaeon *Haloferax volcanii* has split into two elements via homologous recombination. The newly-generated elements are *bona fide* chromosomes, because each bears 'chromosomal' replication origins, rRNA loci and essential genes. The new chromosomes were stable during routine growth but additional genetic manipulation, which involves selective bottlenecks, provoked further rearrangements. To the best of our knowledge, rearrangement of a naturally-evolved prokaryotic genome to generate two new chromosomes has not been described previously.

Introduction

Bacterial genomes usually consist of a single circular chromosome with a unique origin of DNA replication *oriC*, which is recognised by the initiator protein DnaA. Some bacteria, mainly from the phylum Proteobacteria (e.g. *Agrobacterium, Brucella, Rhizobium, Vibrio*), have large secondary replicons termed chromids (Harrison, et al. 2010; diCenzo and Finan 2017). Unlike plasmids, chromids are often comparable to the main chromosome in size and carry core genes that are usually found on the main chromosome. However, in contrast to the main chromosome, chromids have been shown to rely exclusively on plasmid-type DNA replication initiation mechanisms (often in the form of a RepABC system), and not on the DnaA/*oriC* system (Egan, et al. 2005; Pinto, et al. 2012).

Archaea are similar to bacteria in terms of the size and overall organization of their genomes (Koonin and Wolf 2008). However, the core DNA replication proteins found in archaea are more closely related to those of eukaryotes than to their bacterial counterparts. Archaea commonly have more than one origin on the main chromosome and rely on Orc1/Cdc6 replication initiator proteins, which are homologous to the eukaryotic origin recognition complex subunit Orc1 (Makarova and Koonin 2013; Ausiannikava and Allers 2017). Archaeal genomes often have large secondary replicons, which are referred to as mega-plasmids or mini-chromosomes. Unlike bacterial chromids, archaeal mini-chromosomes depend predominantly on Orc1 initiator proteins for their replication, similar to the main chromosome (Ng, et al. 1998; Ng, et al. 2000; Baliga, et al. 2004; Wang, et al. 2015).

Eukaryotic genomes consist of multiple chromosomes that are almost always linear and are each replicated from multiple origins. New extrachromosomal elements arise relatively frequently in eukaryotes (Gaubatz 1990; Moller, et al. 2015; Turner, et al. 2017), but these elements are often transient and low in abundance. Extrachromosomal circular DNAs are common in yeast and may cover up to 23% of the genome (Moller, et al. 2015), and cancer cells often generate highly amplified circular mini-chromosomes called double minute chromosomes (Storlazzi, et al. 2010).

How did multiple chromosomes with multiple origins evolve? The ancestral state is unlikely to have been a single chromosome with a single origin, but it is the simplest one to consider. (i) If present in multiple copies, a single chromosome could diversify by the accumulation of mutations. (ii) More likely, a new element could be acquired by horizontal transfer – over time,

the secondary chromosome would gain core genes from the main chromosome (diCenzo and Finan 2017). (iii) Alternatively, the new element could integrate into the main one, producing a multi-origin chromosome that has the potential to split into two replication-competent chromosomes, thereby giving rise to the state encountered in modern genomes (Egan, et al. 2005; diCenzo and Finan 2017). In bacteria, the presence of plasmid-like replication origins on secondary replicons and the uneven distribution of core genes argues against scenario (i) and in favour of scenario (ii) (Harrison, et al. 2010). Phylogenetic analysis of the multiple replication origins found on archaeal chromosomes indicates that they were independently acquired through horizontal gene transfer and not by duplication of pre-existing origins (Robinson and Bell 2007; Wu, et al. 2012), again apparently ruling out scenario (i) and instead supporting scenario (iii). Because features that are common to all eukaryotic replication origins are elusive, little can be deduced about the evolution of eukaryotic genome organisation but scenario (iii) might be the most parsimonious.

Whatever the evolutionary scenario, genome architecture is not random in prokaryotes (Rocha 2004, 2008; Press, et al. 2016). One of the strongest constraints is the location of replication origins and termination regions; a striking X-shaped pattern of inversions, with endpoints symmetrically located around the origin and terminus of replication, has commonly been observed in bacteria and archaea (Eisen, et al. 2000; Novichkov, et al. 2009; Repar and Warnecke 2017). It has been shown experimentally that altering the size ratio of the two replication arms (replichores) by more than 10% is deleterious for *Escherichia coli* (Esnault, et al. 2007). A strong bias for co-directionality of transcription and replication, which is thought to reduce the collision of RNA and DNA polymerases, also exists in prokaryotic genomes (Wang, et al. 2007; Srivatsan, et al. 2010; Ivanova, et al. 2015). The distribution of repetitive and mobile elements shapes the genome as well, with both homologous and site-specific recombination acting as a potent driving force of chromosome architecture evolution in bacteria and archaea (Brugger, et al. 2004; Papke, et al. 2004; Whitaker, et al. 2005; White, et al. 2008; Bryant, et al. 2012; Cossu, et al. 2017; Mao and Grogan 2017).

Haloferax volcanii, a halophilic archaeon*,* is a tractable model to study prokaryotic genome plasticity and the evolution of new chromosomes (Mullakhanbhai and Larsen 1975; Charlebois, et al. 1991; Hartman, et al. 2010). Its main chromosome has three origins, *oriC1*, *oriC2* and *oriC3* (Norais, et al. 2007; Hawkins, Malla, et al. 2013). Three additional origins exist on the three mini-chromosomes, pHV4, pHV3 and pHV1 (Hartman, et al. 2010). *H.*

volcanii is highly polyploid, with the entire genome present in ~20 copies (Breuert, et al. 2006). Consistent with the highly dynamic nature of archaeal genomes (Redder and Garrett 2006; Bridger, et al. 2012), two cases of genome rearrangements have been detected *in vivo* for *H. volcanii*, namely fusion of the pHV4 mini-chromosome with the main chromosome, and inversion of part of this fused chromosome by recombination between two insertion sequence (IS) elements (Hawkins, Malla, et al. 2013). The former rearrangement has increased the number of replication origins on the main chromosome to four. The involvement of horizontal gene transfer (HGT) in archaeal genome evolution is evident from the presence of many additional copies of replication genes. In the *H. volcanii* genome, there are 16 *orc* genes encoding the Orc1 initiator protein but only 6 origins (Hartman, et al. 2010; Raymann, et al. 2014).

Here we report an unusual genome rearrangement in *H. volcanii*. In our investigation of DNA replication, we generated strains with serial deletions of *orc* genes. It came to our attention that one of these strains had undergone a genome rearrangement. Unexpectedly, the main chromosome split into two parts via homologous recombination between two near-identical *sod* (superoxide dismutase) genes; therefore, it was not due to excision of the integrated pHV4. The two resulting DNA molecules exhibit all the features of *bona fide* chromosomes: they bear replication origins, rRNA loci and essential core genes.

To the best of our knowledge, the evolution of a new chromosome without interspecies HGT has so far not been observed in prokaryotes. Thus, we have witnessed *in vivo* a realisation of the scenario (iii) posited above: a multi-origin chromosome splits into two replication-competent chromosomes. This finding contrasts with our previous report showing fusion of the pHV4 mini-chromosome with the main chromosome (Hawkins, Malla, et al. 2013) and demonstrates that genome rearrangements do not inexorably lead to larger chromosomes. Instead, they can give rise to the multi-origin/multi-chromosome state encountered in modern genomes.

Results

Large-scale genome rearrangement in the strain deleted for Orc1/Cdc6 initiator gene orc5

In our study of Orc1-type initiator proteins and their role in DNA replication in *Haloferax volcanii*, we focussed on the four *orc* genes, *orc1, orc5, orc2* and *orc3*, which are genetically linked to the four chromosomal origins, *oriC1, oriC2, oriC3* and *ori-pHV4*, respectively (Figure 1A). The four origins create eight replichores on the chromosome, with *oriC1* being the most active origin and *ori-pHV4* the least (Hawkins, Malla, et al. 2013). We obtained replication profiles by marker frequency analysis using whole genome sequencing (Muller, et al. 2014). We noted that upon deletion of *orc5* gene, which is located next to *oriC2*, the mutant strain H1689 had acquired large-scale genome rearrangements. This was manifested as two clear discontinuities in the replication profile (indicated by arrows in Figure 1B) (Skovgaard, et al. 2011), when compared to the wild type (WT).

To verify the genome rearrangement by an independent method, we performed restriction digests with *Sfa*AI and analysed the fragment sizes by pulsed field gel electrophoresis (PFGE). We have previously used this method to detect genome rearrangements in *Haloferax volcanii* (Hawkins, Malla, et al. 2013). We observed the disappearance of a band corresponding to a 390 kb fragment, and the appearance of a novel 579 kb fragment in the *Sfa*AI digest of *Δorc5* DNA, confirming a large-scale genome rearrangement (Figure 1C).

New genome architecture of Δorc5 strain

The two interruptions in the replication profile of *Δorc5* mutant (Figure 1B) correspond to the locations of the *sod1* (HVO_A0475; 689201-689803 bp) and *sod2* genes (HVO_2913; 3385084-3385683 bp). The *sod1* and *sod2* superoxide dismutase genes are 603 bp and 600 bp, respectively, and have 100% nucleotide sequence identity (apart from the initial 8 bp); however, their flanking sequences are unique. This provides an opportunity for intrachromosomal homologous recombination of the *sod1* and *sod2* genes, and two outcomes are possible: splitting of the main chromosome into two circular replicons (termed new chr 1 and new chr 2, Figure 2A), or chromosomal inversion of the region between the two *sod* genes. Given that the two *sod* genes are in the same orientation (direct repeats), only the former outcome is possible, as the latter would require the *sod* genes to be arranged as inverted repeats.

To investigate the genome architecture of the Δ*orc5* strain, intact genomic DNA was analysed by PFGE and a Southern blot was probed with *sod1* and *sod2* sequences (Figure 2B). In the wild isolate DS2 (Mullakhanbhai and Larsen 1975), the *sod1* and *sod2* genes are located on pHV4 and the main chromosome, respectively. In the WT laboratory strain H26, pHV4 is fused with the main chromosome and therefore both *sod* genes are on the same molecule (Hawkins, Malla, et al. 2013). In DNA prepared from the Δ*orc5* strain H1689, the *sod1* and *sod2* probes hybridised with two molecules that correspond in size to new chr 1 (2,696 kb) and new chr 2 (787 kb). Using PCR with primers to the unique sequences flanking *sod1* and *sod2*, we determined that these two genes underwent recombination in the Δ*orc5* strain (Figure 2C). DNA sequencing of the PCR products confirmed that the unique flanking sequences of *sod1* and *sod2* had been exchanged in the Δ*orc5* strain.

We constructed maps of the rearranged chromosomes (new chr 1 and new chr 2) and analysed the predicted *sod1/sod2* break points in the *Δorc5* mutant by restriction digests and Southern blotting. As expected, a *Sty*I digest generated one band of 7.8 kb in the WT and a larger 13 kb fragment (plus a faint WT-sized band) in the *Δorc5* strain, which hybridise with a probe adjacent to *sod1* (Figure 3A). Similarly, an *Eco*RV digest of DNA from the WT strain generated a fragment of 8.9 kb, which hybridises with a probe adjacent to *sod2* gene, whereas a smaller 5.5 kb fragment (plus a faint WT-sized band) was seen in the *Δorc5* strain (Figure 3A). The presence of the faint fragment of WT size in both digests of the *Δorc5* mutant suggests that the genome architecture of this strain is not monomorphic, and that the two states (with and without genome rearrangement), coexist in the population.

To confirm the splitting of the chromosome into two circular replicons, genomic DNA was digested with *Sfa*AI, analysed by PFGE and a Southern blot was probed with the *oriC1* downstream region (Figure 3B). In the WT, this probe will hybridise with a fragment of 390 kb that includes *sod2*. If the main chromosome is split into two, the 390 kb fragment will be fused with a 215 kb fragment that includes *sod1*, to generate a product of 579 kb. Such a rearrangement would account for the disappearance of the 390 kb band, and the appearance of a novel 579 kb band, as seen in the *Sfa*AI digest in Figure 1C. The *Sfa*AI-digested *Δorc5* DNA in Figure 3B showed the presence of such a 579 kb band that hybridises with the *oriC1* probe. A faint 390 kb fragment corresponding to the WT was also present in the Δ*orc5* sample, indicating that the genome architecture of this strain is not monomorphic, confirming the observation made in Figure 3A.

To further confirm fragmentation of the chromosome into two replicons, genomic DNA was digested with *Avr*II and *Swa*I, and the fragments were analysed by PFGE (Figure 3C). The two largest *Avr*II fragments of WT are 1,028 kb and 438 kb, and include the *sod2* and *sod1* genes, respectively. When the main chromosome is split into two elements, the largest fragments are 754 kb and 711 kb, and are found on new chr 1 and new chr 2, respectively. The *Avr*II digest of *Δorc5* DNA generated two such fragments of 711 kb and 754 kb, alongside the disappearance of fragments of 1,028 kb and 438 kb. The largest *Swa*I fragments of WT are 1,718 kb, 1,428 kb and 417 kb (the latter is found on pHV3, which is not affected by the genome rearrangement). Splitting the main chromosome into two would eliminate the 1,428 kb *Swa*I fragment and generate a new fragment of 640 kb on new chr 1; these fragments were observed in the *Swa*I digest of *Δorc5* DNA.

Taken together, the PCR and restriction digests indicate that ectopic recombination between the two *sod* genes has led to fragmentation of the main chromosome into two circular replicons. However, the genome architecture of the Δ*orc5* strain is polymorphic; *i.e.* a WT chromosome is still present alongside the two new elements.

***orc5* deletion does not increase rate of large-scale genome rearrangements**

The genome rearrangement in the *Δorc5* strain might have been provoked by asymmetric and unbalanced replichores. In the archaeon *Sulfolobus islandicus*, deletion of *orc1-1* or *orc1-3* genes abolishes replication initiation from the adjacent *oriC1* or *oriC2* origins, respectively (Samson, et al. 2013). A functional linkage of *orc* genes and origins is also found in *H. volcanii*: the replication profile in Figure 1B shows that deletion of *orc5* abolishes replication initiation from *oriC2*, which is adjacent to *orc5*. The replichores that derive from the remaining origins *oriC1*, *oriC3* and *ori-pHV4* are predicted to be highly asymmetrical and unbalanced (Figure 1A vs Figure 4A). Furthermore, in an Δ*orc5* strain, transcription of the rRNA locus that is located adjacent to *oriC2* might no longer proceed in the same direction as DNA replication, provoking head-on collisions of the transcription and replication machinery. Thus, the absence of *orc5* might make the genome unstable and prone to rearrangements. However, the Δ*orc5* strain H1689 shows no major growth defects. The growth rate was determined by competition assay to be 5.5% slower than the WT strain (data not shown). This decrease in growth rate is comparable to the 4% growth defect previously reported for a Δ*oriC2* strain, which does not have a genome rearrangement (Hawkins, Malla, et al. 2013).

To test the effect of asymmetric (unbalanced) replichores, we investigated the scale of genome rearrangements in strains with different combinations of *orc* and origin deletions. A total of 16 additional strains were analysed by *Sfa*AI digestion and PFGE. In all 16 strains, the five largest bands generated by *Sfa*AI were identical in the size to those seen in the WT strain (Figure 4B). Therefore, only the *Δorc5* strain underwent a large-scale genome rearrangement. This rearrangement could have occurred by chance or due to the deletion of *orc5*, which potentially might increase the rearrangement rate.

This hypothesis was tested statistically. As an initial control, we estimated the rate of spontaneous genome rearrangement during *H. volcanii* genome manipulation, by testing 100 independent mutants where the *orc4* gene had been deleted. This gene was chosen because it is not expected to play a role in DNA replication: it is not located next to a replication origin or actively transcribed genes, and as judged by synonymous codon usage, was acquired by HGT (Hartman, et al. 2010). Only 1 of the 100 *Δorc4* clones tested exhibited large-scale genome rearrangements as determined by *Sfa*AI digestion (Figure 4C). The same analysis was conducted with 115 independently-generated *Δorc5* mutants, and only one of the 115 clones tested exhibited a genome rearrangement (Figure 4C). When combined with the Δ*orc5* strain H1689, the estimated rate of large-scale genome rearrangements in the absence of *orc5* is 1.7% (2/116), which is not statistically different from the 1% background rate obtained with *Δorc4* deletion (*p*-value 0.65, chi-squared test). Thus, deletion of *orc5* and any associated change in the size of the replichores does not appear to lead to an increase in large scale genome rearrangements.

Evolution of new chromosomal architecture in Δorc5- derivative strains

In our study of Orc1-type initiator proteins, we generated many strains that were derived from the Δ*orc5* mutant H1689. As we show here, H1689 has a large-scale genome rearrangement but its chromosomal architecture is polymorphic, whereby the two new elements co-exist with the parental chromosome. The genetic manipulation of *H. volcanii* includes selective bottlenecks and extensive propagation (Bitan-Banin, et al. 2003; Allers, et al. 2004), giving an opportunity for polymorphic genome states to be resolved, and potentially for further large-scale rearrangements to occur. Indeed, DNA digests with *Avr*II and *Sfa*AI showed that strains derived from the Δ*orc5* mutant H1689 exhibit notable genome dynamics. We observed fragments corresponding to the WT chromosome, fragments similar to those observed in the *Δorc5* strain H1689, as well as fragments of new sizes (Figure 5A). To determine whether these

new genome fragments had arisen by further recombination between the *sod* genes, we carried out a Southern blot of this region (Figure 5B).

A total of four states were observed in the Δ*orc5* derivatives. (i) In seven strains (lanes 4, 7, 10, 11, 12, 13, 14), additional genome rearrangements were detected by *Avr*II and *Sfa*AI restriction digests (Figure 5A), but these rearrangements did not involve the *sod* gene region (Figure 5B). (ii) Three strains (Figure 5B, lanes 3, 5, 6) had preserved the polymorphic genome architecture of the *Δorc5* strain H1689 (lane 2). (iii) In one strain (lane 8), the genome architecture reverted to the original WT state (lane 1). (iv) In another strain (lane 9), the new chromosomal elements that appeared in the *Δorc5* strain were now present in a monomorphic state. We obtained the replication profile of this monomorphic strain H2202 (*Δorc5 Δorc3*, lane 9). Two clear discontinuities were observed in the same location as those seen previously with the (polymorphic) Δ*orc5* strain H1689 (compare Figure 5C vs Figure 1B).

The replication profile of the Δ*orc5* Δ*orc3* strain H2202 was remapped to sequences corresponding to new chr 1 and new chr 2 (Figure 5D). There is a clear peak at *oriC3* in the profile of new chr 1, which is deleted for *orc5* (adjacent to *oriC2*) but retains *orc2* (adjacent to *oriC3*). Similarly, there is a clear peak at *oriC1* in the profile of new chr 2, which is deleted for *orc3* (adjacent to *ori-pHV4*) but retains *orc1* (adjacent to *oriC1*).

Newly-generated genome elements have features of bona fide chromosomes

To date, six genome elements have been described in *H. volcanii* (Table 1). The original strain DS2 contains the main chromosome, pHV4, pHV3, pHV2 and pHV1 (Charlebois, et al. 1991). The laboratory strain features a new element that was generated by fusion of the main chromosome with pHV4 (Hawkins, Malla, et al. 2013). Here we describe the generation of two new replicons, which result from the fission of the fused main/pHV4 chromosome. This genome rearrangement results from ectopic recombination between the near-identical *sod* genes and not due to excision of the integrated pHV4. Do the new replicons qualify as mega-plasmids, chromids, or mini-chromosomes?

In prokaryotic genomes, chromosomal status is based on the presence of essential and conserved genes, as well as size, copy number, replication control, and evolutionary history (Egan, et al. 2005; Harrison, et al. 2010). We analysed the distribution of these features on the new genome elements. As a measure of evolutionary history, we used synonymous codon usage (SCU) (Hartman, et al. 2010). Local variations in SCU can result from mutation and

selection, but a pronounced bias is usually due to HGT from another species as indicated by a large fraction of rare codons. As a measure of gene conservation, we calculated the fraction of genes on each new chromosome that have been mapped back to the genome of the last archaeal common ancestor (LACA) (Wolf, et al. 2012).

Table 1 indicates that splitting of the fused chromosome generated two replicons that are broadly similar in terms of SCU and the fraction of LACA genes. Both replicons retain an rRNA locus as well as multiple DNA replication origins and *orc* genes. The smaller element retains essential DNA replication genes coding for MCM (HVO_0220), both subunits of polymerase D (HVO_0003, HVO_0065), the large subunit of primase (HVO_0173), PCNA (HVO_0175), and two out of the three subunits of the RFC clamp loader (HVO_0145, HVO_0203); the larger element contains genes coding for polymerase B (HVO_0858), GINS (HVO_2698), the small subunit of primase (HVO_2697), and the histone gene (HVO_0520). Thus, both new genome elements comply with the definition of a chromosome (diCenzo and Finan 2017).

Discussion

The first DNA replication origin to be identified in archaea was described in 2000 for *Pyrococcus abyssi* (Myllykallio, et al. 2000). At the time, it was proposed that archaea and bacteria share a 'standard' prokaryotic genome architecture, comprising a single circular chromosome with a unique origin of replication (Vas and Leatherwood 2000). However, this view was overly simplistic. It has since become clear that archaeal genomes can consist of multiple chromosomes, each with single or multiple origins (Ausiannikava and Allers 2017). This is perhaps best exemplified by the genome architecture of *H. volcanii*, which has one large chromosome with three origins and three mini-chromosomes with one origin each (Table 1). About 10% of bacteria have more than one replicon (diCenzo and Finan 2017), the best studied example being *Vibrio cholerae* which has a large chromosome and a smaller chromid, each with one origin (Jha, et al. 2012). In both *H. volcanii* and *V. cholerae*, genome rearrangements have been documented where two replicons have fused to become one. We have previously reported that during generation of the *H. volcanii* laboratory strain, the pHV4 mini-chromosome fused with the main chromosome by recombination (Hawkins, Malla, et al. 2013). In *V. cholerae*, fusion of the chromosome with the chromid can be induced deliberately or can occur spontaneously. Such spontaneous fusions arise as suppressors of mutations that affect DNA replication (Val, et al. 2014), but naturally-occurring *V. cholerae* strains with a single chromosome have also been reported (Xie, et al. 2017).

Here we describe a genome rearrangement in *H. volcanii* that led to the generation of a new chromosome. The main chromosome, which in the laboratory strain includes the integrated pHV4 mini-chromosome, has split into two parts. The two resulting DNA molecules exhibit all the features of *bona fide* chromosomes: they bear DNA replication origins, rRNA loci and essential core genes. The genome rearrangement that gave rise to the new chromosome was not a simple reversal of the integration of pHV4, which had occurred by recombination between two identical ISH18 insertion sequences (Hawkins, Malla, et al. 2013). Instead, the genome rearrangement reported here occurred via homologous recombination between the near-identical *sod1* and *sod2* genes. In the wild-type, these two genes are located on pHV4 and the main chromosome, respectively, but in the laboratory strain they are located on the same DNA molecule.

Phylogenetic analysis of bacterial genomes indicates that additional chromosomal elements arise relatively rarely but once a viable state is achieved, they remain stable over long

evolutionary intervals (Harrison, et al. 2010; diCenzo and Finan 2017). It is unclear how the stability of the genome is maintained in the multipartite state. Genetic engineering experiments in bacteria have shown that when parts of a multipartite genome are fused, growth rates remain largely unaffected (Guo, et al. 2003; Val, et al. 2012). This finding is consistent with our observation on the absence of a major growth defect in any of the strains described above. However, multipartite genomes have the potential to be highly dynamic because homologous genes are often found on different (or the same) chromosomal elements, providing ample opportunity for recombination.

The constraints on genome architecture, such as the need to coordinate DNA replication with transcription, might be a reason for the observed stability of multipartite genomes. The fission or fusion of genome elements can potentially cause unbalanced replichores (which will be exacerbated by the relocation of replication termination zones), conflicts between replication and transcription, and/or changes in gene dosage. In archaea such as *H. volcanii*, the equidistant location of replication origins on the chromosome could reflect the evolutionary advantage in maintaining such a spatial arrangement. Surprisingly, we observed no immediate effect on genome stability in *H. volcanii* when the replichores are unbalanced. The genome stability was assessed in strains with different combinations of *orc* deletions, and there was no measurable change in the rate of genome rearrangement following deletion of *orc5*. This finding contrasts with bacterial systems, where replichore imbalance has been shown to lead to genome instability and reduced fitness (Esnault, et al. 2007; Dimude, et al. 2016). For example, an *E. coli* strain where the origin was moved to an ectopic site has been found to harbour a large chromosomal inversion (Ivanova, et al. 2015).

Several reasons might account for the lack of deleterious effects of replichore imbalance in *H. volcanii*. (i) In contrast to bacteria, which have discrete *Ter* replication termination sites, archaea and eukaryotes have broad termination zones where converging replication forks meet (Duggin, et al. 2011). This is most likely a consequence of having multiple origins per chromosome, and allows for greater flexibility in replication initiation. (ii) Apart from the highly-transcribed rRNA genes, transcription in *H. volcanii* is not consistently co-orientated with replication (Hartman, et al. 2010). Such an arrangement is both more important and easier to maintain in bacteria, which have a single origin per chromosome. (iii) The polyploid nature of *H. volcanii* genome (where each chromosome is present in 15-20 copies) could also account for the lack of genome instability, because deleterious genome rearrangements can be restored

by gene conversion with a wild-type copy of the affected chromosome. (iv) Little is known about the regulation of replication initiation in archaea. *H. volcanii* might use some origins as a 'backup' to compensate for replichore imbalance, thereby avoiding any potential conflicts. Alternatively, differential origin usage within one cell, where some chromosomes use one origin and others use a different one, would ameliorate unbalanced replichores. Both scenarios – compensatory and stochastic origin firing – have been observed in eukaryotic replication (Hawkins, Retkute, et al. 2013). (v) Recombination-dependent replication, which is used in the absence of origins, leads to dispersed initiation throughout the genome and may relieve the spatial constraints on replication origins. Thus, replichore imbalance would have only minor effects on the viability of *H. volcanii*.

Nonetheless, it is notable that the Δ*orc5*-derivative strains exhibited considerable genome plasticity and the ability to evolve to different chromosome architectures (Figure 5). The two new chromosomes were stable during routine growth but new rounds of genetic manipulation appeared to provoke further rearrangements. Following transformation, a selectable marker will initially be present on only one of the 20 chromosome copies. This selectable marker will then spread throughout the genome by gene conversion, and may carry with it genetically-linked rearrangements. Therefore, the selective bottleneck of genetic manipulation might allow a new chromosome architecture to become monomorphic.

Eukaryotic cells contain multiple linear chromosomes that are replicated from multiple origins. For this type of genome architecture to arise, three steps are required (but not necessarily in this order): multiplication of origins, multiplication of chromosomes, and linearisation of chromosomes. Given the shared evolutionary history of eukaryotes and archaea, it is not surprising that two of these three features are found in archaeal genomes as well. Up to four replication origins can be present on some archaeal chromosomes, and multiple chromosomes that use an Orc-type replication initiation mechanism co-exist in haloarchaeal species; however, no archaeon with linear chromosomes has been found to date. Here we show that an increase in the number of circular chromosomes is easily achievable through natural evolution. To the best of our knowledge, rearrangement of a naturally-evolved prokaryotic genome that generates two new chromosomes, each with pre-existing multiple origins that depend on the same type of replication initiation, has not been described previously. Interestingly, the *H. volcanii* genome might already contain an imprint of a similar event, where the ancestral chromosome fragmented leading to the generation of a new chromosome. Indeed, the pHV3

mini-chromosome has one Orc-dependent replication origin, a native SCU and GC content similar to the main chromosome, and a high proportion of LACA genes (Table 1); thus, the generation of pHV3 is compatible with the recombinational route described here.

Newly-generated chromosomal elements must find effective solutions for segregation and replication, and the ability to spread throughout a population would be beneficial. Haloarchaea have developed potential solutions to these challenges. The proclivity of *H. volcanii* to use recombination-dependent replication in the absence of origins weakens the requirement for newly-generated chromosomal elements to maintain balanced replichores, or even origins (Hawkins, Malla, et al. 2013). *H. volcanii* does not strictly depend on orderly segregation of its chromosomes, because its genome is highly polyploid and new chromosomal elements can rely on random partitioning into daughter cells; furthermore, archaea lack the centromeres found on eukaryotic chromosomes. Haloarchaea have a remarkable capacity for rapid genome evolution by HGT. The exchange of up to 530 kb of DNA between different *Haloferax* species has been detected after cell fusion (Naor, et al. 2012), thus providing the opportunity for a newly-generated chromosome (and eventually, a new species) to arise. And because archaeal origins are nearly always linked to an *orc* gene encoding their cognate initiator protein, a 'foreign' chromosome will be efficiently replicated in its new host cell. The remarkable plasticity of haloarchaeal genomes thus presents a test bed for probing the evolution of genome organisation and replication initiation.

Materials and Methods

Strains and plasmids

H. volcanii strains (Table 2) were grown at 45°C on complete (Hv-YPC) or casamino acids (Hv-Ca) agar, or in Hv-YPC broth, as described previously (Allers, et al. 2004). Isolation of genomic and plasmid DNA, and transformation of *H. volcanii*, were carried out as described previously (Allers, et al. 2004). Standard molecular techniques were used (Sambrook and Russell 2001). Deletion mutants were constructed and confirmed by colony hybridisation and/or Southern blotting as described previously (Allers, et al. 2004). Plasmids for gene deletion are shown in Table 3 and were generated by PCR using oligonucleotides shown in Table 4. Probes for Southern blots are shown in Table 5. Growth competition assays were carried out as described previously (Hawkins, Malla, et al. 2013).

Screening for genome rearrangements in Δorc5 and Δorc4-deleted backgrounds

Twelve independent 'pop-in' strains were generated using Δ*orc5* and Δ*orc4* plasmids pTA1375 and pID19T-HVO_2042, respectively, and ten deletion ('pop-out') strains were derived from each 'pop-in'. Gene deletions were confirmed by colony hybridisation with the relevant *orc5* or *orc4* probes. The deletion strains were assessed for *Sfa*AI restriction fragment length polymorphisms by pulsed field gel electrophoresis.

Marker frequency analysis by deep sequencing

For exponential-phase samples, strains were grown overnight in Hv-YPC broth, diluted 500-fold in fresh media and incubated at 45°C with vigorous aeration until an A650 of 0.4, then diluted 500-fold in fresh media and grown until an A650 of 0.2. For a stationary-phase sample, a wild-type culture was grown at 45°C for 3 days until saturation (no further increase in A650). Genomic DNA was isolated from 50 ml cultures followed by phenol:chloroform extraction as described previously (Hawkins, Malla, et al. 2013). Marker frequency analysis was performed by Deep Seq (University of Nottingham) using Illumina HiSeq 2000 sequencing to measure sequence copy number. Enrichment of uniquely mapping sequence tags was calculated (in 1-kb windows) for exponentially growing samples relative to a stationary phase wild-type sample, to correct for differences in read depth across the genome (Skovgaard, et al. 2011; Muller, et al. 2014). Sequence reads were mapped to the *H. volcanii* genome and replication profiles were calculated as described previously (Hawkins, Malla, et al. 2013).

Pulsed field gel electrophoresis

For pulsed field gel electrophoresis (PFGE), genomic DNA was prepared in agarose plugs and digested as described previously (Hawkins, Malla, et al. 2013). For analysis of intact genomic DNA, agarose plugs were subjected to 100 Gy of γ radiation using a ^{137}Cs source (Gammacell 1000), to linearise circular chromosomes (Beverley 1989). PFGE was performed using a CHEF Mapper apparatus (Bio-Rad). Intact and *Sfa*AI-digested DNA fragments were separated on a 1.2% agarose gel in 0.5X TBE at 14°C, with a gradient voltage of 6 V/cm, linear ramping, an included angle of 120°, initial and final switch times of 0.64 sec and 1 min 13.22 sec, respectively, and a run time of 40 hr (intact DNA) or 20 hr 46 min (*Sfa*AI-digested DNA). *Avr*II-digested and *Swa*I-digested genomic DNA were separated on 1% agarose gel in 0.5X TBE at 14°C, with a gradient voltage of 6 V/cm, linear ramping, an included angle of 120°, initial and final switch times of 1 min and 2 min, respectively, and a run time of 24 hr. The gel was stained with ethidium bromide.

List of abbreviations

IS: insertion sequence; HGT: horizontal gene transfer; WT: wild type; PFGE: pulsed field gel electrophoresis; SCU: synonymous codon usage; LACA: last archaeal common ancestor.

Declarations

Availability of data and material

Sequencing datasets generated and analysed during this study are available in the NCBI Gene Expression Omnibus under accession number GSE108201.

Competing interests

The authors declare that there are no competing interests.

Funding

This work was supported by the Biotechnology and Biological Sciences Research Council (BBSRC) [grant number BB/M001393/1]. The funders had no role in study design, data collection and interpretation, or the decision to submit the work for publication.

Author contributions

DA and TA conceived the study and wrote the manuscript with input from all authors. DA, LM, HM and TA performed the genetic experiments. MH generated the Δ*orc5* strain H1689. VS performed the PFGE in Figure 1C. CN analysed the DNA replication profiles. KM and EK analysed the LACA gene distribution. All authors read and approved the manuscript.

Acknowledgements

We thank Uri Gophna and Nathan Jones for helpful comments on the manuscript, Sunir Malla (Deep Seq, Nottingham) for DNA sequencing, Christopher Turley for assistance with PFGE in Figure 4, and Jerry Eichler (Ben Gurion University, Israel) for the Δ*orc4::trpA*$^{+}$ plasmid pID19T-HVO_2042.

References

Allers T, Ngo HP, Mevarech M, Lloyd RG. 2004. Development of additional selectable markers for the halophilic archaeon Haloferax volcanii based on the leuB and trpA genes. Appl Environ Microbiol 70:943-953.

Ausiannikava D, Allers T. 2017. Diversity of DNA Replication in the Archaea. Genes (Basel) 8.

Baliga NS, Bonneau R, Facciotti MT, Pan M, Glusman G, Deutsch EW, Shannon P, Chiu Y, Weng RS, Gan RR, et al. 2004. Genome sequence of Haloarcula marismortui: a halophilic archaeon from the Dead Sea. Genome Res 14:2221-2234.

Beverley SM. 1989. Estimation of circular DNA size using gamma-irradiation and pulsed-field gel electrophoresis. Anal Biochem 177:110-114.

Bitan-Banin G, Ortenberg R, Mevarech M. 2003. Development of a gene knockout system for the halophilic archaeon Haloferax volcanii by use of the pyrE gene. J Bacteriol 185:772-778.

Breuert S, Allers T, Spohn G, Soppa J. 2006. Regulated polyploidy in halophilic archaea. PLoS One 1:e92.

Bridger SL, Lancaster WA, Poole FL, 2nd, Schut GJ, Adams MW. 2012. Genome sequencing of a genetically tractable Pyrococcus furiosus strain reveals a highly dynamic genome. J Bacteriol 194:4097-4106.

Brugger K, Torarinsson E, Redder P, Chen L, Garrett RA. 2004. Shuffling of Sulfolobus genomes by autonomous and non-autonomous mobile elements. Biochem Soc Trans 32:179-183.

Bryant J, Chewapreecha C, Bentley SD. 2012. Developing insights into the mechanisms of evolution of bacterial pathogens from whole-genome sequences. Future Microbiol 7:1283-1296.

Charlebois RL, Schalkwyk LC, Hofman JD, Doolittle WF. 1991. Detailed physical map and set of overlapping clones covering the genome of the archaebacterium Haloferax volcanii DS2. J Mol Biol 222:509-524.

Cossu M, Badel C, Catchpole R, Gadelle D, Marguet E, Barbe V, Forterre P, Oberto J. 2017. Flipping chromosomes in deep-sea archaea. PLoS Genet 13:e1006847.

diCenzo GC, Finan TM. 2017. The Divided Bacterial Genome: Structure, Function, and Evolution. Microbiol Mol Biol Rev 81.

Dimude JU, Midgley-Smith SL, Stein M, Rudolph CJ. 2016. Replication Termination: Containing Fork Fusion-Mediated Pathologies in Escherichia coli. Genes (Basel) 7.

Duggin IG, Dubarry N, Bell SD. 2011. Replication termination and chromosome dimer resolution in the archaeon Sulfolobus solfataricus. EMBO J 30:145-153.

Egan ES, Fogel MA, Waldor MK. 2005. Divided genomes: negotiating the cell cycle in prokaryotes with multiple chromosomes. Mol Microbiol 56:1129-1138.

Eisen JA, Heidelberg JF, White O, Salzberg SL. 2000. Evidence for symmetric chromosomal inversions around the replication origin in bacteria. Genome Biol 1:RESEARCH0011.

Esnault E, Valens M, Espeli O, Boccard F. 2007. Chromosome structuring limits genome plasticity in Escherichia coli. PLoS Genet 3:e226.

Gaubatz JW. 1990. Extrachromosomal circular DNAs and genomic sequence plasticity in eukaryotic cells. Mutat Res 237:271-292.

Guo X, Flores M, Mavingui P, Fuentes SI, Hernandez G, Davila G, Palacios R. 2003. Natural genomic design in Sinorhizobium meliloti: novel genomic architectures. Genome Res 13:1810-1817.

Harrison PW, Lower RP, Kim NK, Young JP. 2010. Introducing the bacterial 'chromid': not a chromosome, not a plasmid. Trends Microbiol 18:141-148.

Hartman AL, Norais C, Badger JH, Delmas S, Haldenby S, Madupu R, Robinson J, Khouri H, Ren Q, Lowe TM, et al. 2010. The complete genome sequence of Haloferax volcanii DS2, a model archaeon. PLoS One 5:e9605.

Hawkins M, Malla S, Blythe MJ, Nieduszynski CA, Allers T. 2013. Accelerated growth in the absence of DNA replication origins. Nature 503:544-547.

Hawkins M, Retkute R, Muller CA, Saner N, Tanaka TU, de Moura AP, Nieduszynski CA. 2013. High-resolution replication profiles define the stochastic nature of genome replication initiation and termination. Cell Rep 5:1132-1141.

Ivanova D, Taylor T, Smith SL, Dimude JU, Upton AL, Mehrjouy MM, Skovgaard O, Sherratt DJ, Retkute R, Rudolph CJ. 2015. Shaping the landscape of the Escherichia coli chromosome: replication-transcription encounters in cells with an ectopic replication origin. Nucleic Acids Res 43:7865-7877.

Jha JK, Baek JH, Venkova-Canova T, Chattoraj DK. 2012. Chromosome dynamics in multichromosome bacteria. Biochim Biophys Acta 1819:826-829.

Koonin EV, Wolf YI. 2008. Genomics of bacteria and archaea: the emerging dynamic view of the prokaryotic world. Nucleic Acids Res 36:6688-6719.

Lestini R, Duan Z, Allers T. 2010. The archaeal Xpf/Mus81/FANCM homolog Hef and the Holliday junction resolvase Hjc define alternative pathways that are essential for cell viability in Haloferax volcanii. DNA Repair (Amst) 9:994-1002.

Makarova KS, Koonin EV. 2013. Archaeology of eukaryotic DNA replication. Cold Spring Harb Perspect Biol 5:a012963.

Mao D, Grogan DW. 2017. How a genetically stable extremophile evolves: Modes of genome diversification in the archaeon Sulfolobus acidocaldarius. J Bacteriol.

Moller HD, Parsons L, Jorgensen TS, Botstein D, Regenberg B. 2015. Extrachromosomal circular DNA is common in yeast. Proc Natl Acad Sci U S A 112:E3114-3122.

Mullakhanbhai MF, Larsen H. (76060741 co-authors). 1975. *Halobacterium volcanii* spec. nov., a Dead Sea halobacterium with a moderate salt requirement. Arch Microbiol 104:207-214.

Muller CA, Hawkins M, Retkute R, Malla S, Wilson R, Blythe MJ, Nakato R, Komata M, Shirahige K, de Moura AP, et al. 2014. The dynamics of genome replication using deep sequencing. Nucleic Acids Res 42:e3.

Myllykallio H, Lopez P, Lopez-Garcia P, Heilig R, Saurin W, Zivanovic Y, Philippe H, Forterre P. 2000. Bacterial mode of replication with eukaryotic-like machinery in a hyperthermophilic archaeon. Science 288:2212-2215.

Naor A, Lapierre P, Mevarech M, Papke RT, Gophna U. 2012. Low species barriers in halophilic archaea and the formation of recombinant hybrids. Curr Biol 22:1444-1448.

Ng WV, Ciufo SA, Smith TM, Bumgarner RE, Baskin D, Faust J, Hall B, Loretz C, Seto J, Slagel J, et al. 1998. Snapshot of a large dynamic replicon in a halophilic archaeon: megaplasmid or minichromosome? Genome Res 8:1131-1141.

Ng WV, Kennedy SP, Mahairas GG, Berquist B, Pan M, Shukla HD, Lasky SR, Baliga NS, Thorsson V, Sbrogna J, et al. 2000. Genome sequence of Halobacterium species NRC-1. Proc Natl Acad Sci U S A 97:12176-12181.

Norais C, Hawkins M, Hartman AL, Eisen JA, Myllykallio H, Allers T. 2007. Genetic and physical mapping of DNA replication origins in Haloferax volcanii. PLoS Genet 3:e77.

Novichkov PS, Wolf YI, Dubchak I, Koonin EV. 2009. Trends in prokaryotic evolution revealed by comparison of closely related bacterial and archaeal genomes. J Bacteriol 191:65-73.

Papke RT, Koenig JE, Rodriguez-Valera F, Doolittle WF. 2004. Frequent recombination in a saltern population of Halorubrum. Science 306:1928-1929.

Pinto UM, Pappas KM, Winans SC. 2012. The ABCs of plasmid replication and segregation. Nat Rev Microbiol 10:755-765.

Press MO, Queitsch C, Borenstein E. 2016. Evolutionary assembly patterns of prokaryotic genomes. Genome Res 26:826-833.

Raymann K, Forterre P, Brochier-Armanet C, Gribaldo S. 2014. Global phylogenomic analysis disentangles the complex evolutionary history of DNA replication in archaea. Genome Biol Evol 6:192-212.

Redder P, Garrett RA. 2006. Mutations and rearrangements in the genome of Sulfolobus solfataricus P2. J Bacteriol 188:4198-4206.

Repar J, Warnecke T. 2017. Non-random inversion landscapes in prokaryotic genomes are shaped by heterogeneous selection pressures. Mol Biol Evol.

Robinson NP, Bell SD. 2007. Extrachromosomal element capture and the evolution of multiple replication origins in archaeal chromosomes. Proc Natl Acad Sci U S A 104:5806-5811.

Rocha EP. 2008. Evolutionary patterns in prokaryotic genomes. Curr Opin Microbiol 11:454-460.

Rocha EP. 2004. Order and disorder in bacterial genomes. Curr Opin Microbiol 7:519-527.

Sambrook J, Russell DW. 2001. Molecular cloning : a laboratory manual. Cold Spring Harbor, N.Y.: Cold Spring Harbor Laboratory Press.

Samson RY, Xu Y, Gadelha C, Stone TA, Faqiri JN, Li D, Qin N, Pu F, Liang YX, She Q, et al. 2013. Specificity and function of archaeal DNA replication initiator proteins. Cell Rep 3:485-496.

Skovgaard O, Bak M, Lobner-Olesen A, Tommerup N. 2011. Genome-wide detection of chromosomal rearrangements, indels, and mutations in circular chromosomes by short read sequencing. Genome Res 21:1388-1393.

Srivatsan A, Tehranchi A, MacAlpine DM, Wang JD. 2010. Co-orientation of replication and transcription preserves genome integrity. PLoS Genet 6:e1000810.

Storlazzi CT, Lonoce A, Guastadisegni MC, Trombetta D, D'Addabbo P, Daniele G, L'Abbate A, Macchia G, Surace C, Kok K, et al. 2010. Gene amplification as double minutes or homogeneously staining regions in solid tumors: origin and structure. Genome Res 20:1198-1206.

Turner KM, Deshpande V, Beyter D, Koga T, Rusert J, Lee C, Li B, Arden K, Ren B, Nathanson DA, et al. 2017. Extrachromosomal oncogene amplification drives tumour evolution and genetic heterogeneity. Nature 543:122-125.

Val ME, Skovgaard O, Ducos-Galand M, Bland MJ, Mazel D. 2012. Genome engineering in Vibrio cholerae: a feasible approach to address biological issues. PLoS Genet 8:e1002472.

Val ME, Soler-Bistue A, Bland MJ, Mazel D. 2014. Management of multipartite genomes: the Vibrio cholerae model. Curr Opin Microbiol 22:120-126.

Vas A, Leatherwood J. 2000. Where does DNA replication start in archaea? Genome Biol 1:REVIEWS1020.

Wang H, Peng N, Shah SA, Huang L, She Q. 2015. Archaeal extrachromosomal genetic elements. Microbiol Mol Biol Rev 79:117-152.

Wang JD, Berkmen MB, Grossman AD. 2007. Genome-wide coorientation of replication and transcription reduces adverse effects on replication in Bacillus subtilis. Proc Natl Acad Sci U S A 104:5608-5613.

Whitaker RJ, Grogan DW, Taylor JW. 2005. Recombination shapes the natural population structure of the hyperthermophilic archaeon Sulfolobus islandicus. Mol Biol Evol 22:2354-2361.

White JR, Escobar-Paramo P, Mongodin EF, Nelson KE, DiRuggiero J. 2008. Extensive genome rearrangements and multiple horizontal gene transfers in a population of pyrococcus isolates from Vulcano Island, Italy. Appl Environ Microbiol 74:6447-6451.

Wolf YI, Makarova KS, Yutin N, Koonin EV. 2012. Updated clusters of orthologous genes for Archaea: a complex ancestor of the Archaea and the byways of horizontal gene transfer. Biol Direct 7:46.

Wu Z, Liu H, Liu J, Liu X, Xiang H. 2012. Diversity and evolution of multiple orc/cdc6-adjacent replication origins in haloarchaea. BMC Genomics 13:478.

Xie G, Johnson SL, Davenport KW, Rajavel M, Waldminghaus T, Detter JC, Chain PS, Sozhamannan S. 2017. Exception to the Rule: Genomic Characterization of Naturally Occurring Unusual *Vibrio cholerae* Strains with a Single Chromosome. Internat J Genomics 2017:8724304.

Figure Legends

Figure 1

Genome rearrangement of *Δorc5* strain. **A.** Location of replication origins and adjacent *orc* genes on *H. volcanii* main chromosome (+pHV4). Positions of the two rRNA loci are indicated with black arrows. The integrated pHV4 mini-chromosome is indicated by a thick line. The eight replichores representing the direction of replication forks are shown by coloured arrows, corresponding to their respective origins. *Sfa*AI sites are indicated by tick marks. **B.** Replication profiles of the Δ*orc5* mutant H1689 and a reference wild-type (WT) laboratory strain H26. The number of reads is plotted against the chromosomal location. The linearized *H. volcanii* chromosome showing positions of *oriC* and *orc genes* is shown below (coloured as in Figure 1A). Two discontinuities in the *Δorc5* replication profile are indicated by vertical arrows. **C.** Restriction fragment length polymorphisms in WT and *Δorc5* strain as shown by digestion with *Sfa*AI and PFGE. The 390 kb *Sfa*AI fragment (shown on the map in panel A) is absent from the digest of *Δorc5* DNA, and a novel 579 kb *Sfa*AI fragment is present; these bands are indicated by arrows.

Figure 2

Novel genome architecture of *Δorc5* strain. **A.** Scheme for outcome of recombination between *sod1* and *sod2* genes to split the main chromosome (+pHV4) and generate two new chromosomes (new chr 1 and new chr 2). **B.** PFGE and Southern blot confirming two new chromosomes in Δ*orc5* strain. Intact genomic DNA of wild isolate DS2, WT H26 and *Δorc5* H1689 strains was probed with *sod1* and *sod2* sequences. **C.** Recombination of *sod1* and *sod2* genes in Δ*orc5* strain H1689 was confirmed by end-point PCR using primers to unique sequences flanking *sod1* and *sod*. The identity of the PCR products was validated by DNA sequencing.

Figure 3

Genome architecture of the Δ*orc5* strain is polymorphic. **A.** Southern blot conforming location of breakpoints of genome rearrangement in Δ*orc5* strain. Genomic DNA of WT H26 and *Δorc5* H1689 was digested with *Sty*I or *Eco*RV and probed with sequences adjacent to *sod1* or *sod2*, respectively. A WT-sized band is present in the *Δorc5* lanes. **B.** Southern blot of PFGE confirming relocation of *oriC1* to new chr 2 in Δ*orc5* strain. *Sfa*AI-digested DNA of WT H26

and *Δorc5* H1689 strains was probed with sequences adjacent to *oriC1*. Relevant *Sfa*AI sites are indicated on the maps, the new chr 1 does not hybridise with *oriC1* (map not shown). A faint 390 kb WT-sized band is present in the *Δorc5* lane. **C.** PFGE confirming new genome architecture of *Δorc5* strain. Genomic DNA of WT H26 and *Δorc5* H1689 was digested with *Avr*II or *Swa*I. Relevant *Avr*II and *Swa*I sites are indicated on the outside and inside of chromosome maps, respectively. The 417 bp *Swa*I fragment is found on pHV3 (not shown), which is not affected by the genome rearrangement.

Figure 4

Deletion of *orc5* does not increase the rate of genome rearrangement. **A.** Scheme showing new replichores in the absence of *orc5* (replichores and rRNA loci indicated as in Figure 1A). **B.** *Sfa*AI restriction fragment length polymorphisms were not seen in unrelated strains with different combinations of *orc* and *oriC* deletion. Strain genotypes are indicated below. **C.** *Sfa*AI-digested genomic DNA of 25 independently-derived *Δorc4* mutants and 25 independently-derived *Δorc5* mutants. Representative images, the *Δorc4* clone and *Δorc5* clone with a genome rearrangement are indicated by an asterisk.

Figure 5

New genome architectures of Δ*orc5* derivatives. **A.** *Avr*II and *Sfa*AI digests of genomic DNA from derivatives of *Δorc5* strain H1689 identifying four different genome states. Strain genotypes and genome architecture state is indicated below, polymorphic and monomorphic refer to strains with H1689-type genome rearrangements. The monomorphic *Δorc5 Δorc3* strain H2202 is indicated. **B.** Southern blots showing that additional genome rearrangements in derivatives of Δ*orc5* strain H1689 did not involve recombination of the *sod* gene region. Genomic DNA was digested with *Sty*I or *Eco*RV and probed with sequences adjacent to *sod1* or *sod2*, respectively (for key to restriction fragments, see Figure 3A). **C.** Replication profile of *Δorc5 Δorc3* strain H2202 (lane 9 in panels A and B) where the genome is in a monomorphic state. Labelled as in Figure 1B, the two discontinuities in the replication profile are indicated by vertical arrows. **D.** Replication profile of *Δorc5 Δorc3* strain H2202 remapped to sequences corresponding to new chr 1 and new chr 2.

Table 1. *Distribution of features on genome elements in H. volcanii wild isolate DS2, laboratory strain H26 and Δorc5 strain H1689*

Strain(s)	Genome element	Size, bp	Number of genes	SCU, rare codons	GC content	LACA genes	rRNA loci	Replication origins
DS2	Chromosome	2847757	2960	7.3%	66.6%	37.3%	2	*oriC1, oriC2, oriC3*
DS2	pHV4	635786	636	15.5%	61.7%	28.3%	0	*ori-pHV4*
H26	Chromosome + pHV4	3482975	3596	8.7%	65.7%	35.5%	2	*oriC1, oriC2, oriC3, ori-pHV4*
H1689	New chr1	2695880	2781	8.3%	66.1%	37.4%	1	*oriC2, oriC3*
H1689	New chr2	787095	815	10.3%	64.6%	33%	1	*oriC1, ori-pHV4*
DS2, H26, H1689	pHV3	437906	380	7.7%	65.5%	35.9%	0	*ori-pHV3*
DS2, H26, H1689	pHV1	85092	88	26.3%	55.5%	18%	0	*ori-pHV1*

New genomic elements generated by fission of the fused chromosome + pHV4 are designated as New chr1 and New chr2. The fraction of rare codons was calculated from SCU tables for each genome element (Hartman, et al. 2010). The fraction of LACA genes was calculated with cut-off probability of 0.75 (Wolf, et al. 2012).

Table 2. *H. volcanii strains*

Strain	Genotype	Derivation	Use
DS2		(Mullakhanbhai and Larsen 1975)	Wild isolate
H26	Δ*pyrE2*	(Allers, et al. 2004)	Standard laboratory strain
H53	Δ*pyrE2* Δ*trpA*	(Allers, et al. 2004)	Laboratory strain, *trpA* deletion
Strains with large-scale genome rearrangements			
H1689	Δ*pyrE2* Δ*orc5*	H26 pTA1375	Deletion of *orc5*, large-scale genome rearrangement
H1822	Δ*pyrE2* Δ*orc5* Δ*trpA*	H1689 pTA95	*trpA* deletion in Δ*orc5* strain
H2149	Δ*pyrE2* Δ*orc5* Δ*orc9*	H1689 pTA1433	*orc9* deletion in Δ*orc5* strain
H2196	Δ*pyrE2* Δ*orc5* Δ*orc1*	H1689 pTA1610	*orc1* deletion in Δ*orc5* strain
H2202	Δ*pyrE2* Δ*orc5* Δ*orc3*	H1689 pTA1373	*orc3* deletion in Δ*orc5* strain
H2313	Δ*pyrE2* Δ*orc5* Δ*trpA* Δ*orc2::trpA+*	H1822 pTA1632	*orc2* deletion in Δ*orc5* strain
H2458	Δ*pyrE2* Δ*orc5* Δ*orc3* Δ*orc9*	H2202 pTA1433	*orc9* deletion in Δ*orc5* Δ*orc3* strain
H2459	Δ*pyrE2* Δ*orc5* Δ*orc1* Δ*orc9*	H2196 pTA1433	*orc9* deletion in Δ*orc5* Δ*orc1* strain

H2562	Δ*pyrE2* Δ*orc5* Δ*orc9* Δ*orc2*	H2149 pTA1379	*orc2* deletion in Δ*orc5* Δ*orc9* strain
H2733	Δ*pyrE2* Δ*orc5* Δ*orc3* Δ*trpA*	H2202 pTA95	*trpA* deletion in Δ*orc5* Δ*orc3* strain
H2738	Δ*pyrE2* Δ*orc5* Δ*orc3* Δ*orc9* Δ*trpA*	H2458 pTA95	*trpA* deletion in Δ*orc5* Δ*orc3* Δ*orc9* strain
H2786	Δ*pyrE2* Δ*orc5* Δ*orc9* Δ*trpA*	H2149 pTA95	*trpA* deletion in Δ*orc5* Δ*orc9* strain
H3195	Δ*pyrE2* Δ*orc5 p.tnaA-radA+*	H1689 pTA1837	Tryptophan-inducible *radA* allele in Δ*orc5* strain

Strains with wild-type genome architecture

H1691	Δ*pyrE2* Δ*orc2*	H26 pTA1379	Deletion of *orc2*
H1829	Δ*pyrE2* Δ*orc4::trpA+*	H53 pTA1452	Deletion of *orc4*
H2197	Δ*pyrE2* Δ*orc1* Δ*orc2*	H2199 pTA1610	*orc2* deletion in Δ*orc1* strain
H2199	Δ*pyrE2* Δ*orc1*	H26 pTA1610	Deletion of *orc1*
H2203	Δ*pyrE2* Δ*orc2* Δ*orc3*	H1691 pTA1373	*orc3* deletion in Δ*orc2* strain
H2304	Δ*pyrE2* Δ*orc3* Δ*ori-pHV4*	H26 pTA1631	Deletion of *ori-pHV4* and *orc3*
H2305	Δ*pyrE2* Δ*orc1* Δ*orc2* Δ*orc5*	H2197 pTA1375	*orc5* deletion in Δ*orc1* Δ*orc2* strain

H2308	Δ*pyrE2* Δ*orc2* Δ*orc3* Δ*orc5*
H2312	Δ*pyrE2* Δ*orc2* Δ*orc5*
H2413	Δ*pyrE2* Δ*orc1* Δ*orc2* Δ*orc5* Δ*orc3*
H2490	Δ*pyrE2* Δ*orc3* Δ*ori-pHV4* Δ*orc2 oriC3*
H2492	Δ*pyrE2* Δ*orc2* Δ*oriC3*
H2494	Δ*pyrE2* Δ*orc1* Δ*oriC1*
H2497	Δ*pyrE2* Δ*orc3* Δ*ori-pHV4* Δ*orc1* Δ*oriC1*
H2560	Δ*pyrE2* Δ*orc2* Δ*oriC3* Δ*orc1* Δ*oriC1*
H2561	Δ*pyrE2* Δ*orc2* Δ*oriC3* Δ*orc3* Δ*ori-pHV4* Δ*orc1* Δ*oriC1*
H2578	Δ*pyrE2* Δ*orc1* Δ*oriC1* Δ*orc5* Δ*oriC2*
H2579	Δ*pyrE2* Δ*orc5* Δ*oriC2*
H2581	Δ*pyrE2* Δ*orc2* Δ*oriC3* Δ*orc3* Δ*ori-pHV4* Δ*orc5* Δ*oriC2*

H2203 pTA1375	*orc5* deletion in Δ*orc2* Δ*orc3* strain
H1691 pTA1375	*orc5* deletion in Δ*orc2* strain
H2305 pTA1373	*orc3* deletion in Δ*orc1* Δ*orc2* Δ*orc5* strain
H2304 pTA1692	*oriC3* and *orc2* deletion in Δ*ori-pHV4* Δ*orc3* strain
H26 pTA1692	Deletion of *oriC3* and *orc2*
H26 pTA1691	Deletion of *oriC1* and *orc1*
H2304 pTA1691	*oriC1* and *orc1* deletion in Δ*ori-pHV4* Δ*orc3* strain
H2492 pTA1691	*oriC1* and *orc1* deletion in Δ*oriC3* Δ*orc2* strain
H2490 pTA1691	*oriC1* and *orc1* deletion in Δ*oriC3* Δ*orc2* Δ*ori-pHV4* Δ*orc3* strain
H2494 pTA1712	*oriC2* and *orc5* deletion in Δ*oriC1* Δ*orc1* strain
H26 pTA1712	Deletion of *oriC2* and *orc5*
H2490 pTA1712	*oriC2* and *orc5* deletion in Δ*oriC3* Δ*orc2* Δ*ori-pHV4* Δ*orc3* strain

H2656	Δ*pyrE2* Δ*orc1* Δ*oriC1* Δ*orc2* Δ*oriC3* Δ*orc3* Δ*ori-pHV4* Δ*orc5* Δ*oriC2*	H2561 pTA1712	*oriC2* and *orc5* deletion in Δ*oriC1* Δ*orc1* Δ*oriC3* Δ*orc2* Δ*ori-pHV4* Δ*orc3* strain
H2658	Δ*pyrE2* Δ*orc1* Δ*oriC1* Δ*orc2* Δ*oriC3* Δ*orc5* Δ*oriC2*	H2560 pTA1712	*oriC2* and *orc5* deletion in Δ*oriC1* Δ*orc1* Δ*oriC3* Δ*orc2* strain
H2729	Δ*pyrE2* Δ*orc3* Δ*ori-pHV4* Δ*orc5* Δ*oriC2*	H2579 pTA1631	*ori-pHV4* and *orc3* deletion in Δ*oriC2* Δ*orc5* strain
H2870	Δ*pyrE2* Δ*orc3*	H26 pTA1373	Deletion of *orc3*
H3380	Δ*pyrE2* Δ*trpA* Δ*orc5::trpA+*	H53 pTA1633	Deletion of *orc5*

Table 3. *Plasmids*

Plasmid	Relevant properties	Derivation
pTA95	Integrative plasmid for *trpA* gene deletion	(Allers, et al. 2004)
pTA131	Integrative plasmid based on pBluescript II, with *pyrE2*$^{+}$ marker	(Allers, et al. 2004)
pTA298	pUC19 with *trpA*$^{+}$ marker flanked by *Bam*HI sites	(Lestini, et al. 2010)
pTA333	pUC19 with *Sac*I-*Nsp*I chromosomal fragment containing *orc4* gene	This study
pTA415	pBluescript II SK+ with *Mlu*I chromosomal fragment containing *hel308* helicase gene	This study
pTA416	pBluescript II with *Sac*I chromosomal fragment containing *orc5* and *oriC2*	(Norais, et al. 2007)
pTA419	pTA131 with *Nhe*I-*Eco*RI fragment of pTA416 containing *orc5* and *oriC2*	This study
pTA1100	pBluescript II with *Aci*I chromosomal fragment containing *orc2* and *oriC3*	(Hawkins, Malla, et al. 2013)
pTA1329	pTA131 with Δ*ori-pHV4* construct	(Hawkins, Malla, et al. 2013)

pTA1343	pTA131 with *p.tnaA-radA*$^{+}$*::hdrB*$^{+}$ construct flanked by upstream and downstream *radA* regions	(Hawkins, Malla, et al. 2013)
pTA1370	pBluescript II SK+ with *Hind*III-*Kpn*I chromosomal fragment containing *orc1* gene and *oriC1* origin	This study
pTA1371	pBluescript II SK+ with *BstB*I chromosomal fragment containing *orc3* gene	This study
pTA1373	pTA131 with Δ*orc3* construct, comprising *Cla*I-*Bam*HI fragment of upstream flanking region of *orc3* and *Bam*HI-*Xba*I fragment of downstream flanking region of *orc3,* PCR amplified from pTA1371	This study
pTA1375	pTA131 with Δ*orc5* construct, comprising *Kpn*I-*Bam*HI fragment of downstream flanking region of *orc5* and *Bam*HI-*Xba*I fragment of upstream flanking region of *orc5*, PCR amplified from pTA416	This study
pTA1379	pTA131 with Δ*orc2* construct, comprising *Kpn*I-*Bam*HI upstream flanking region of *orc2* and *Bam*HI-*Xba*I fragment of downstream flanking region of *orc2,* PCR amplified from pTA1100	This study
pTA1431	pTA131 with inactivation of unique *Bam*HI site in MCS by filling-in with Klenow	This study
pTA1432	pBluescript II SK+ with *Not*I chromosomal fragment containing *orc9* gene	This study
pTA1433	pTA1431 with Δ*orc9* construct, comprising *Xba*I-*Bst*XI upstream flanking region of *orc9* and *Xba*I-*Bst*XI fragment of downstream flanking region of *orc9,* PCR amplified from pTA1432	This study
pTA1610	pTA131 with Δ*orc1* construct, comprising *Kpn*I-*Bam*HI upstream flanking region of *orc1* and *Bam*HI-*Xho*I fragment of downstream flanking region of *orc1,* PCR amplified from pTA1370	This study
pTA1631	Δ*orc3* Δ*ori-pHV4* construct, where *orc3* upstream region of pTA1373 was replaced by *Kpn*I-*Bam*HI fragment of *ori-pHV4* upstream region from pTA1329	This study

pTA1632	pTA1379 with insertion of *Bam*HI *trpA*$^+$ fragment from pTA298	This study
pTA1633	pTA1375 with insertion of *Bam*HI *trpA*$^+$ fragment from pTA298	This study
pTA1691	pTA131 with Δ*orc1* Δ*oriC1* construct, comprising *Stu*I-*Bam*HI upstream flanking region of *oriC1* and *Bam*HI-*Xba*I fragment of downstream flanking region of *orc1,* PCR amplified from pTA1370	This study
pTA1692	pTA131 with Δ*orc2* Δ*oriC3* construct, comprising *Aat*II-*Bam*HI upstream flanking region of *oriC3* and *Bam*HI-*Kpn*I fragment of downstream flanking region of *orc2,* PCR amplified from pTA1100	This study
pTA1712	pTA131 with Δ*orc5* Δ*oriC2* construct, comprising *Xba*I-*Bam*HI upstream flanking region of *oriC2* and *Bam*HI-*Xba*I fragment of downstream flanking region of *orc5,* PCR amplified from pTA416	This study
pTA1837	pTA131 with *p.tnaA-radA*$^+$ construct. *Xba*I-*Bam*HI fragment of *hdrB*$^+$ marker was removed from pTA1343, and 890 bp *Eco*RV-*Pvu*II fragment of *radA* upstream flanking region (PCR amplified from H26 genomic DNA) was used to replace 315 bp *Eco*RV-*Pvu*II fragment of *radA* upstream flanking region in pTA1343	This study
pID19T-HVO_2042	pTA131 with Δ*orc4::trpA*$^+$ construct, comprising *Xho*I-*Hind*III fragment of upstream flanking region of *orc4* and *Bam*HI-*Xba*I fragment of downstream flanking region of *orc4*, PCR amplified from H26 genomic DNA, joined using *Hind*III-*Bam*HI *trpA*$^+$ fragment	Jerry Eichler

Table 4. *Oligonucleotides*

Primer	Sequence (5'–3')	Relevant properties	Use
MHorc3F1	CGTTCAtCGATTTGACGAGGTCATCCACG	*orc3* deletion, upstream	pTA1373
MHorc3R1	GTCCCGGaTCCCGATAGATCTCGGTGTCC	*orc3* deletion, upstream	pTA1373
MHorc3F2	ACGACTggATCcAGCAGTAGGTAGGTCG	*orc3* deletion, downstream	pTA1373
MHorc3R2	CCTCCGtCtAGAACACGACGTGCGCGACC	*orc3* deletion, downstream	pTA1373
MHorc2F1	CAGCGgTAcCGACCCGTCGCAGAGGTACG	*orc2* deletion, upstream	pTA1379
MHorc2R1	CGCAGGatCCGAGGCCGCCTGACCCCACG	*orc2* deletion, upstream	pTA1379
MHorc2F2	GCTCGgAtCCGGCGCATTAGCGTCGGTCC	*orc2* deletion, downstream	pTA1379, pTA1692
MHorc2R2	CCGAGGTctAGACATTTCGAGGGGCGG	*orc2* deletion, downstream	pTA1379, pTA1692
MHorc5F1	GTGCTAGGTacCTGAACACCCATAAGTG	*orc5/oriC2orc5* deletions, downstream	pTA1375, pTA1712
MHorc5R1	GCTCGAGGATCCGGACGTGGTGAGGGACG	*orc5/oriC2orc5* deletions, downstream	pTA1375, pTA1712
MHorc5F2	GTGAAGAGGaTCcTCGCTGGCGTTAGGC	*orc5* deletion, upstream	pTA1375
MHorc5R2	GGGGAAtcTAGAGAACCGGAAAACCCGG	*orc5* deletion, upstream	pTA1375

delorc9USR	TCTTCGGGaTCCTCCCTCATCGAG	*orc9* deletion, upstream	pTA1433
delorc9DSF	CGGTCGgAtCCGCGCCATCTCGCTCG	*orc9* deletion, downstream	pTA1433
pBSR3	ACCCCAGGCTTTACACTTTATGC	*orc9* deletion, downstream	pTA1433
pBSF2	TTAAGTTGGGTAACGCCAGGG	*orc9* deletion, upstream, and *oriC1orc1* deletion, downstream	pTA1433, pTA1691
MHorc1F1	ACGAGCgGTaCCGGACGATGCGCGCCGGC	*orc1* deletion, downstream	pTA1610
dorc1DF	AGAACGggaTCCCGAAGTCCGACGC	*orc1*/*oriC1orc1* deletion, downstream	pTA1610, pTA1691
MHorc1F2	GTTCCCGGaTCCCCTCGTGCGCCGCCTCG	*orc1* deletion, upstream	pTA1610
MHorc1R2	CCACAGTCTaGaCCTCGCCGCAGTAGCCG	*orc1* deletion, upstream	pTA1610
oriC1-BamHL	GTACTCCGGATCCATGCTCGGTATCCG	*oriC1orc1* deletion, upstream	pTA1691
pBSR2	CGCGCAATTAACCCTCACTAAAG	*oriC1orc1* and *oriC3orc2* deletions, upstream	pTA1691, pTA1692
oriC3-BamHL	GGTGTCGGAtCcCGGCTTTCGCGTTCCG	*oriC3orc2* deletion, upstream	pTA1692
OriC2-BamL	CCGGTCTCGGATCCAACTTAGCTCTCACTCG	*oriC2orc5* deletion, upstream	pTA1712
OriC2-XbaR	CGACCCTCTAGAGCGAGGCGAGGTCGCCCC	*oriC2orc5* deletion, upstream	pTA1712
5'HVO_2042_XhoI_F	cccctcgagTCTTTGCAGTCTATTTCCTTC	*orc4* deletion, upstream	pID19T-HVO_2042

5'HVO_2042_HindIII_R	gggaagcttACGTGTTGCAGACCTGTATAC	*orc4* deletion, upstream	pID19T-HVO_2042
3'HVO_2042_BamHI_F	cccggatccCCCACAGAACAGATGAAGTG	*orc4* deletion, downstream	pID19T-HVO_2042
3'HVO_2042_XbaI_R	gggtctagaCGTGCTTCCGAGTCAGAAAC	*orc4* deletion, downstream	pID19T-HVO_2042
radAUSNdeR	TTCTGCCATAtgCAGTCGTTCCGCCTATACCC	*p.tnaA:radA*+ construct, upstream	pTA1837
radAextraUS	AGACCAGCTGAGTTCCGATGGGGCTGTTC	*p.tnaA:radA*+ construct, upstream	pTA1837
sod1F	AGTACAGGCCGAACTCGACGACGCC	*sod1* Southern blot probe, diagnostic PCR and sequencing of *sod1*	Figure 2B, 2C
sod1R	TCTCACGGTAACCTGTGGTCGCGCG	*sod1* Southern blot probe, diagnostic PCR and sequencing of *sod1*	Figure 2B, 2C
sod2F	GAAATCGCCGACGCCGTCTCGACG	*sod2* Southern blot probe, diagnostic PCR and sequencing of *sod2*	Figure 2B, 2C
sod2R	GAGCAGTTTCGGACCTTCGTCGGCG	*sod2* Southern blot probe, diagnostic PCR and sequencing of *sod2*	Figure 2B, 2C
sod1 US-left	ACAGGCTCCGAACGTATCAT	*sod1U* Southern blot probe	Figures 3A, 5B
sod1 US-right	CAGTCGGTGAGTCCCTGTAA	*sod1U* Southern blot probe	Figures 3A, 5B
sod2 DS-left	GATGACCTCCGCGACCTC	*sod2D* Southern blot probe	Figures 3A, 5B
sod2 DS-right	GGGTCGCTGAACAGGTCC	*sod2D* Southern blot probe	Figures 3A, 5B

Table 5. *Probes*

Probe	Usage	Location	Source
sod1	Figure 2B	*sod1* gene	813 bp PCR using sod1F and sod1R
sod2	Figure 2B	*sod2* gene	1074 bp PCR using sod2F and sod2R
sod1U	Figure 3A, Figure 5B	Upstream of *sod1* gene	359 bp PCR using sod1 US-left and sod1 US-right
sod2D	Figure 3A, Figure 5B	Downstream of *sod2* gene	347 bp PCR using sod2 DS-left and sod2 DS-right
oriC1	Figure 3B	Downstream of *oriC1* origin	763 bp *Sty*I fragment of pTA415
orc4	Confirmation of *orc4* deletion by colony hybridisation	*orc4* gene	959 bp *Bgl*II-*Pst*I fragment of pTA333
orc5	Confirmation of *orc5* deletion by colony hybridisation	*orc5* gene	784 bp *Aat*II fragment of pTA419

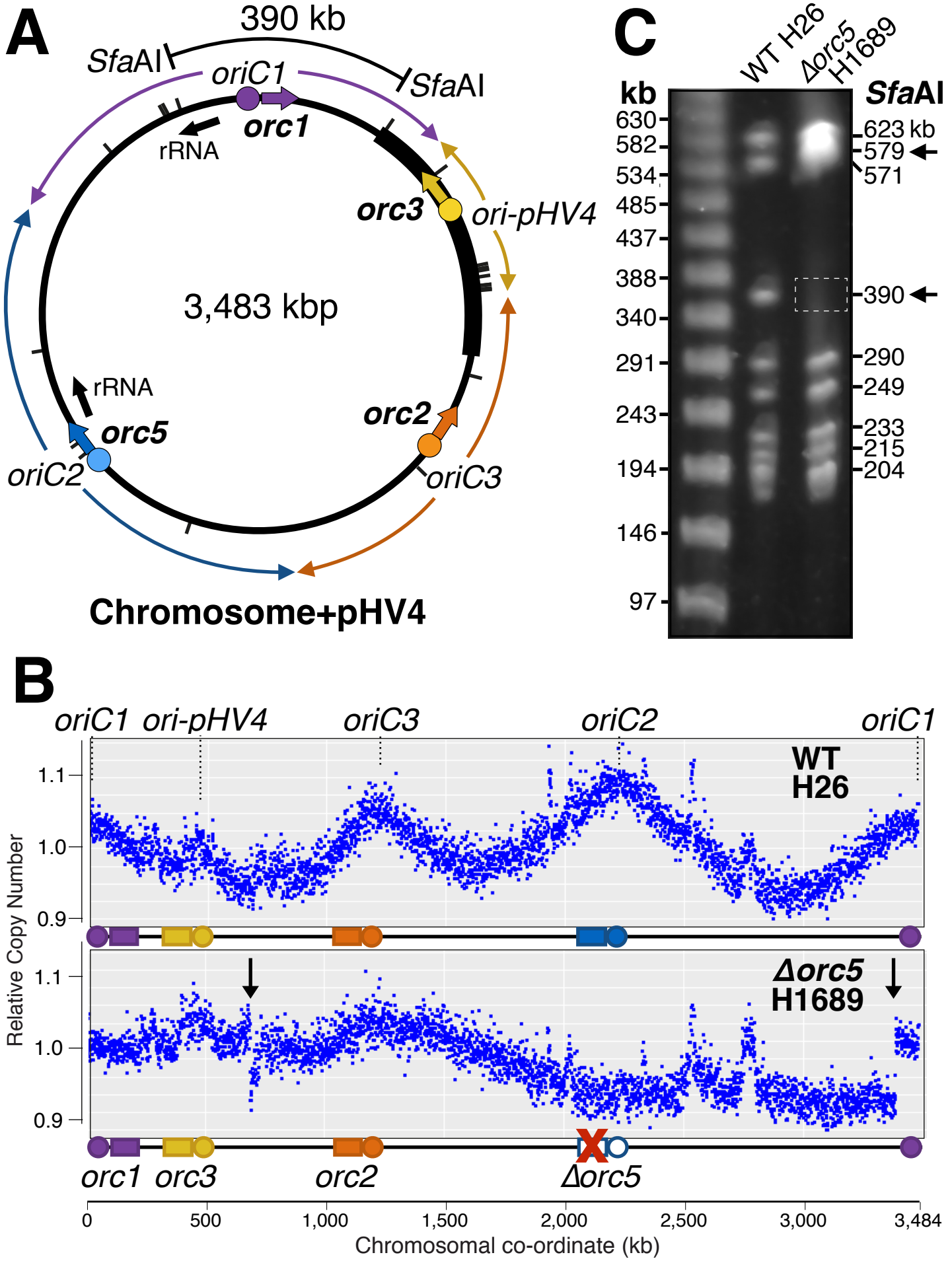

Figure 1

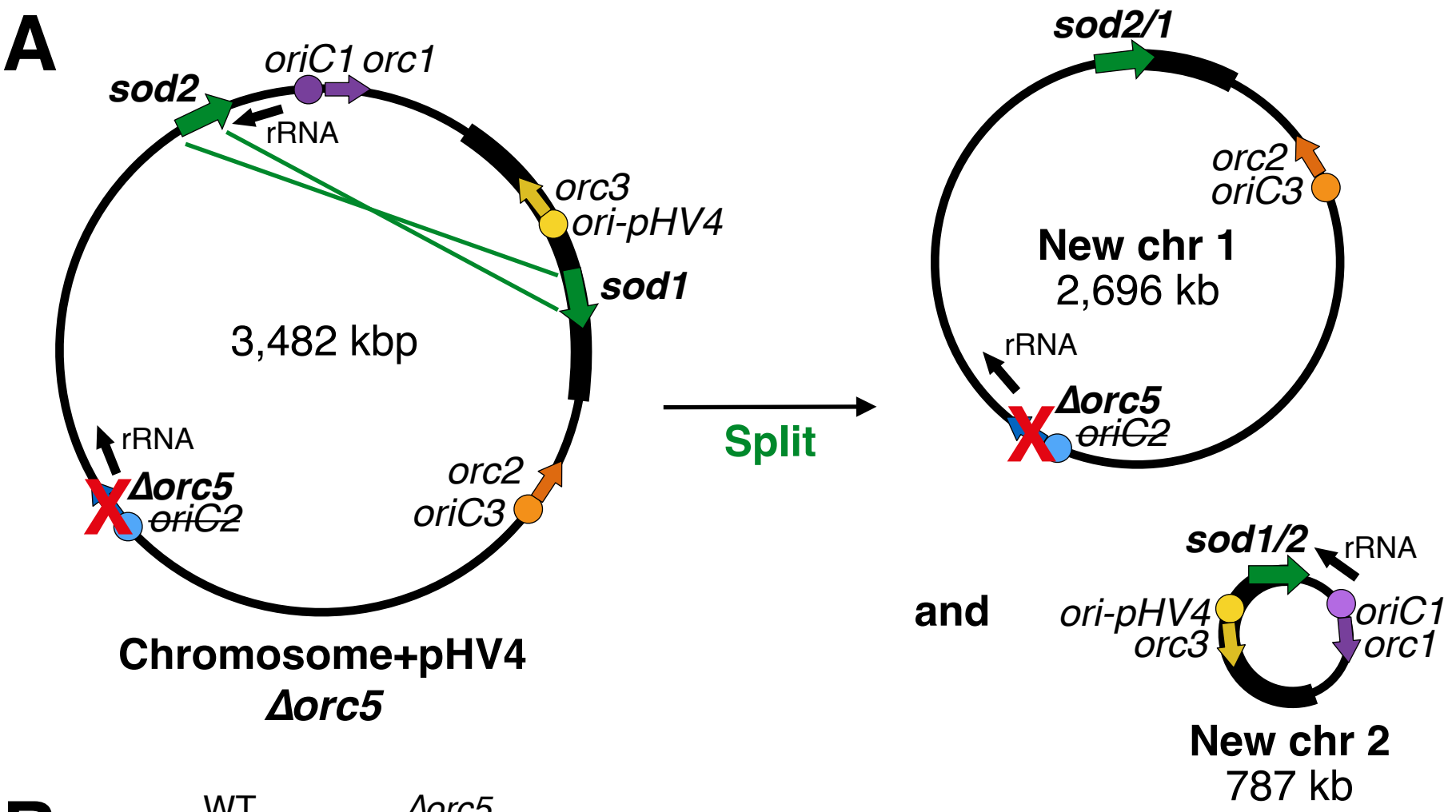

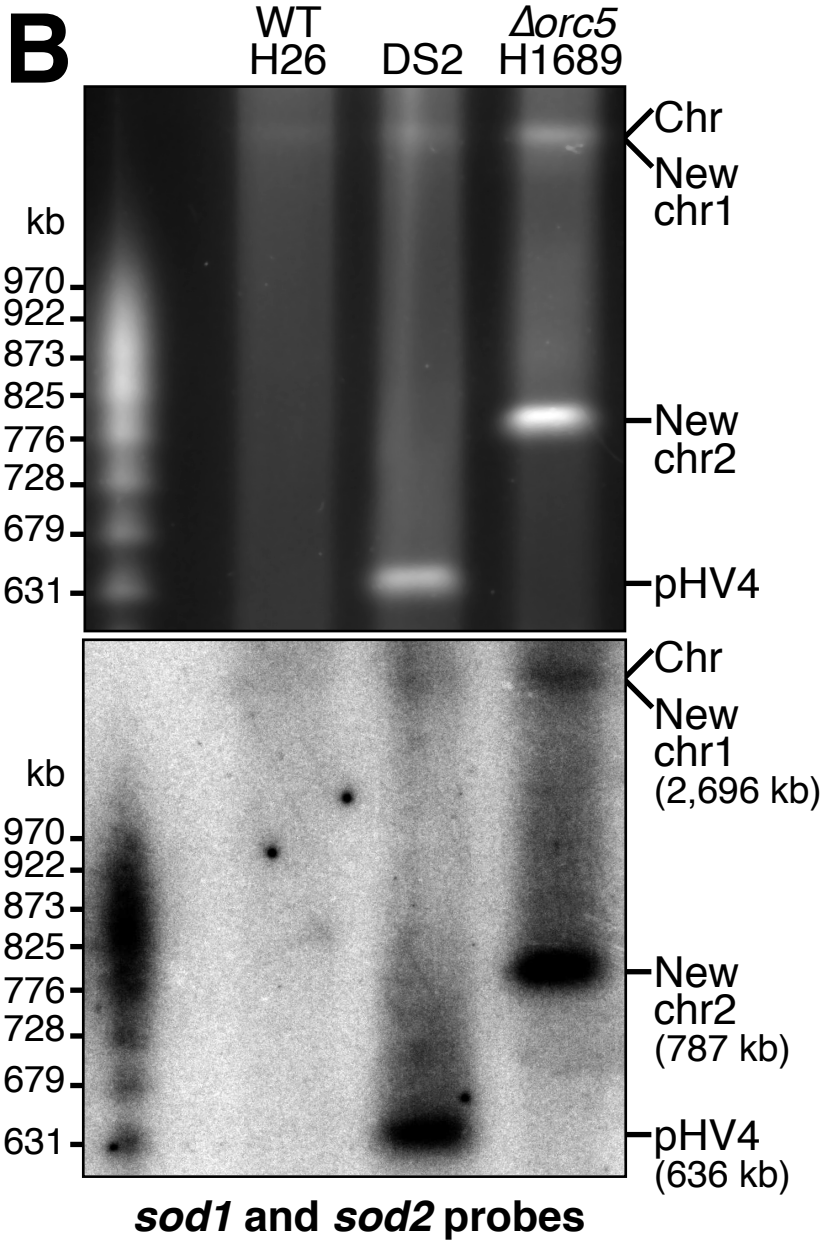

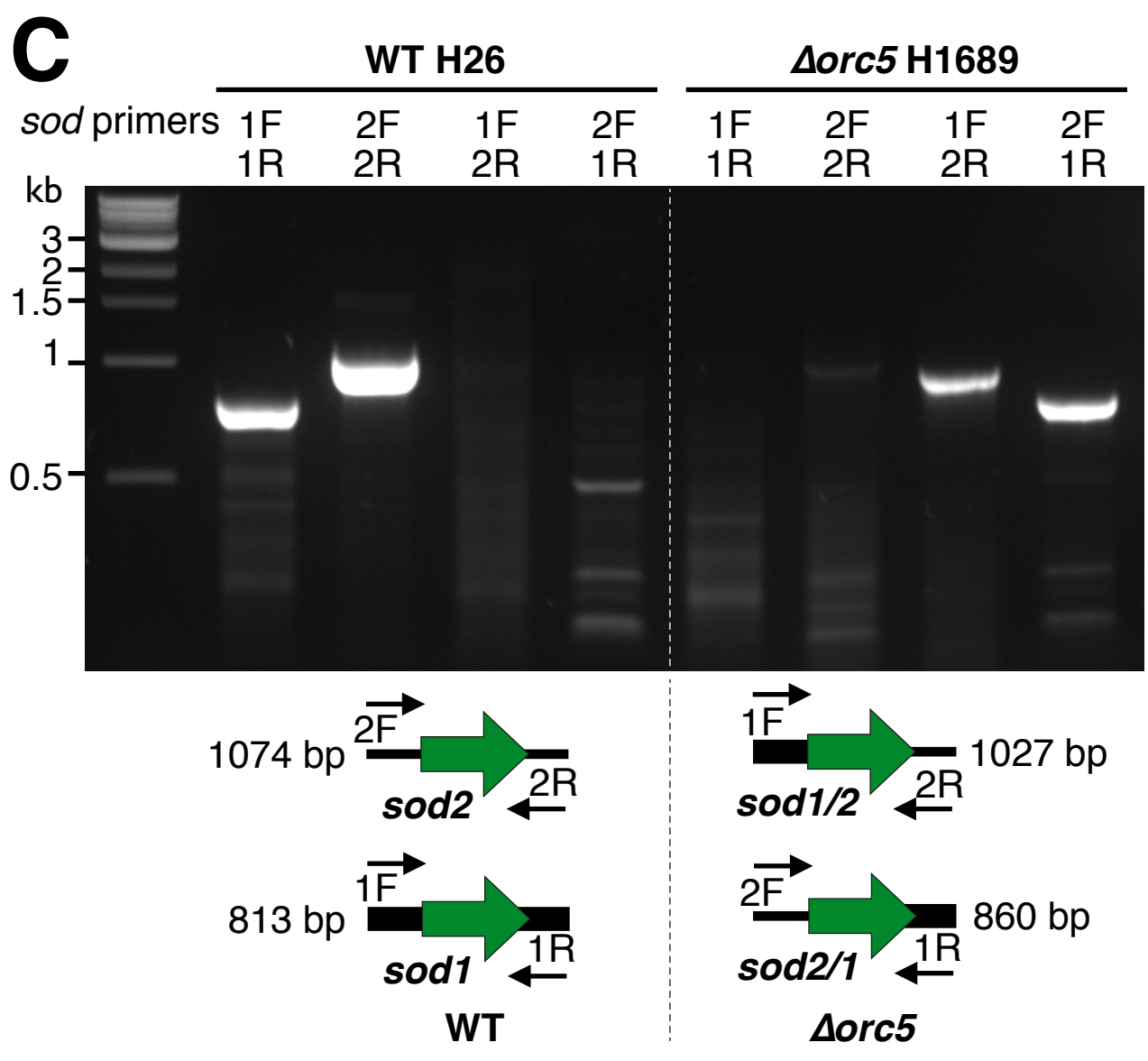

Figure 2

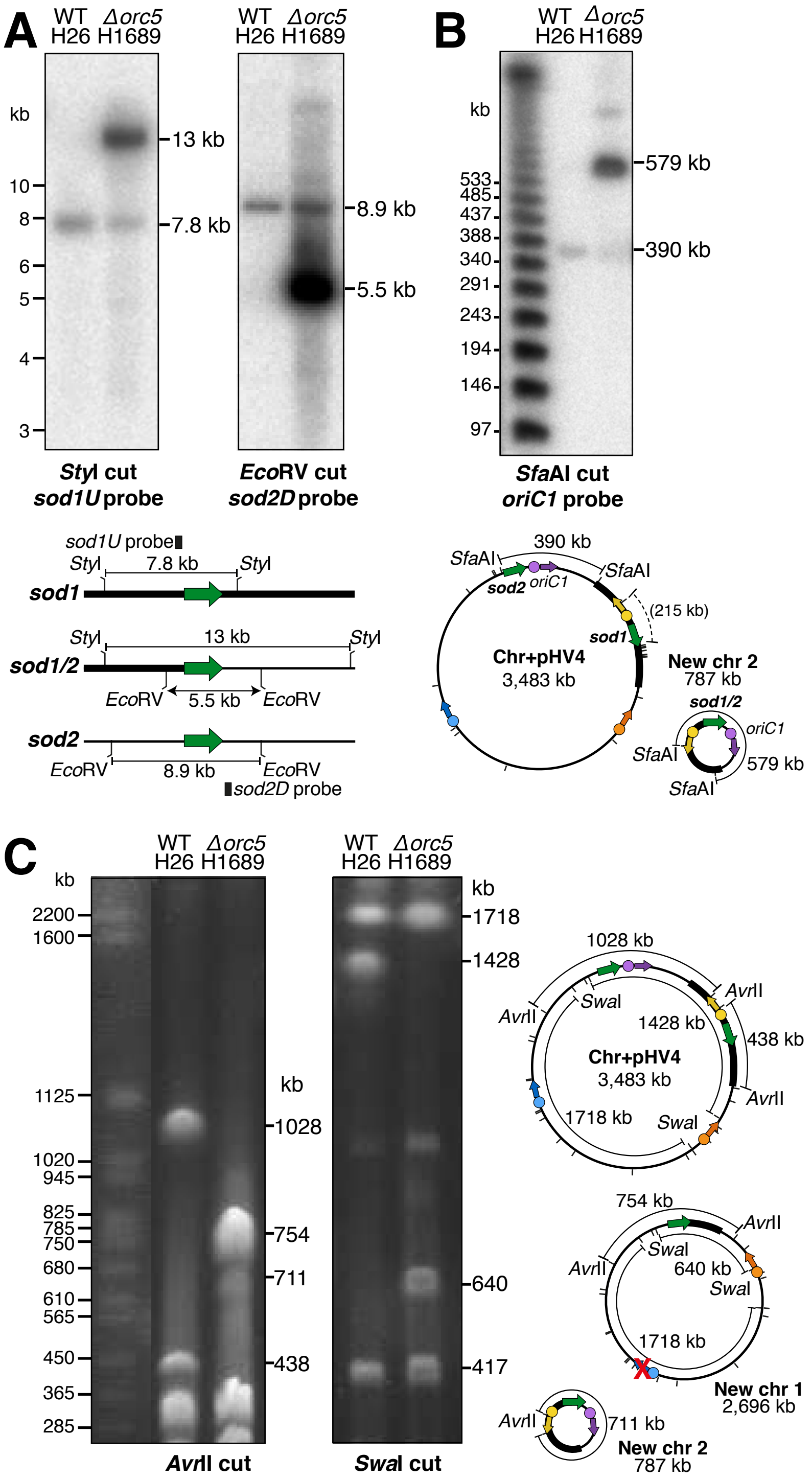

Figure 3

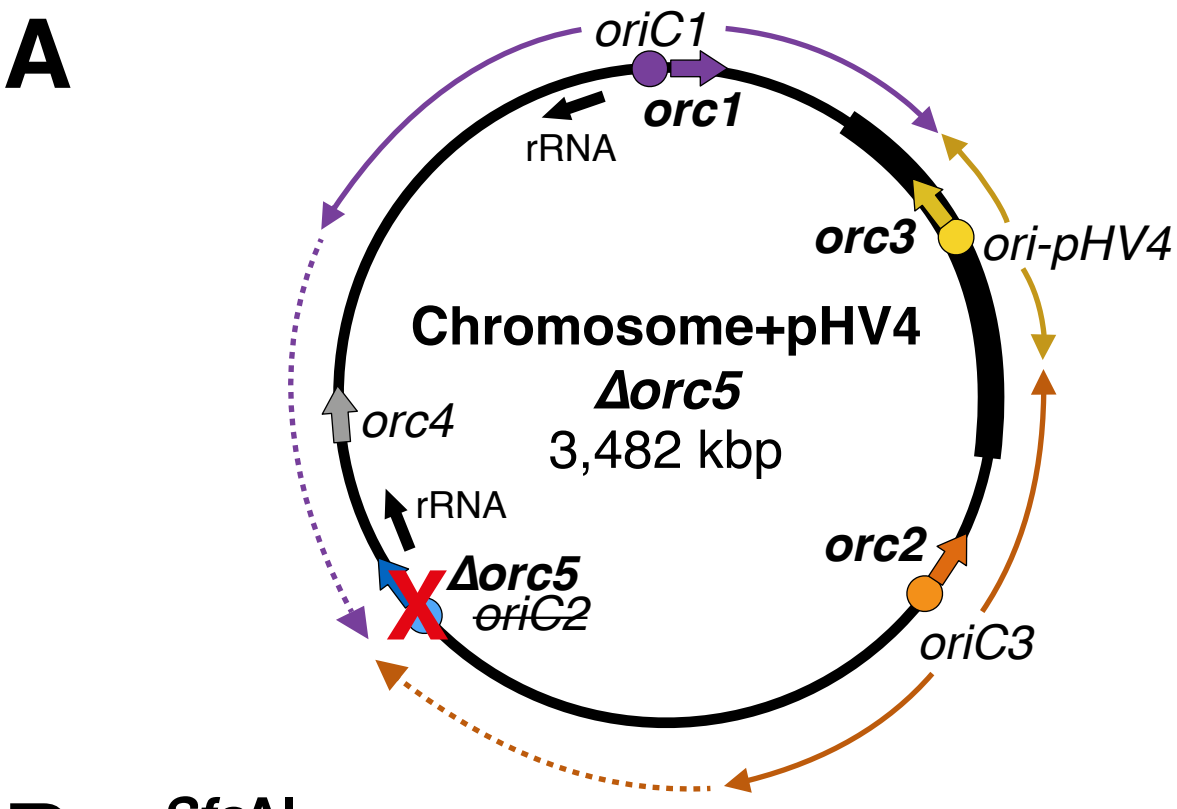

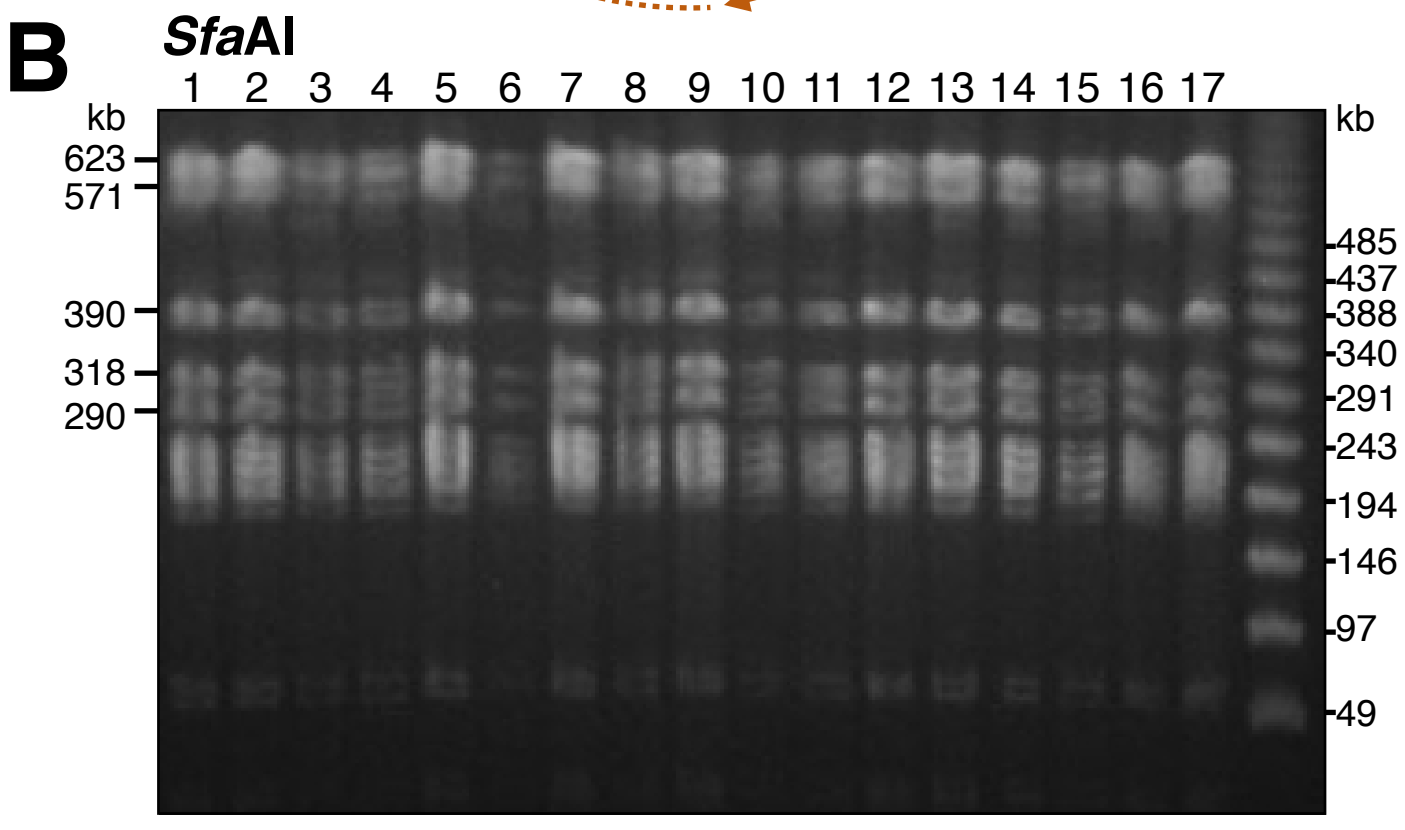

1. H1691 *Δorc2*
2. H1829 *Δorc2 Δorc1*
3. H2199 *Δorc1*
4. H2305 *Δorc1 Δorc2 Δorc5*
5. H2308 *Δorc2 Δorc3 Δorc5*
6. H2312 *Δorc2 Δorc5*
7. H2413 *Δorc1 Δorc2 Δorc5 Δorc3*
8. H2490 *Δorc2 ΔoriC3 Δorc3 Δori-pHV4*
9. H2497 *Δorc1 ΔoriC1 Δorc3 Δori-pHV4*
10. H2560 *Δorc1 ΔoriC1 Δorc2 ΔoriC3*
11. H2578 *Δorc1 ΔoriC1 Δorc5 ΔoriC2*
12. H2581 *Δorc2 ΔoriC3 Δorc5 ΔoriC2 Δorc3 Δori-pHV4*
13. H2656 *Δorc1 ΔoriC1 Δorc2 ΔoriC3 Δorc5 ΔoriC2 Δorc3 Δori-pHV4*
14. H2658 *Δorc1 ΔoriC1 Δorc2 ΔoriC3 Δorc5 ΔoriC2*
15. H2729 *Δorc5 ΔoriC2 Δorc3 Δori-pHV4*
16. H2870 *Δorc3*
17. H26 WT

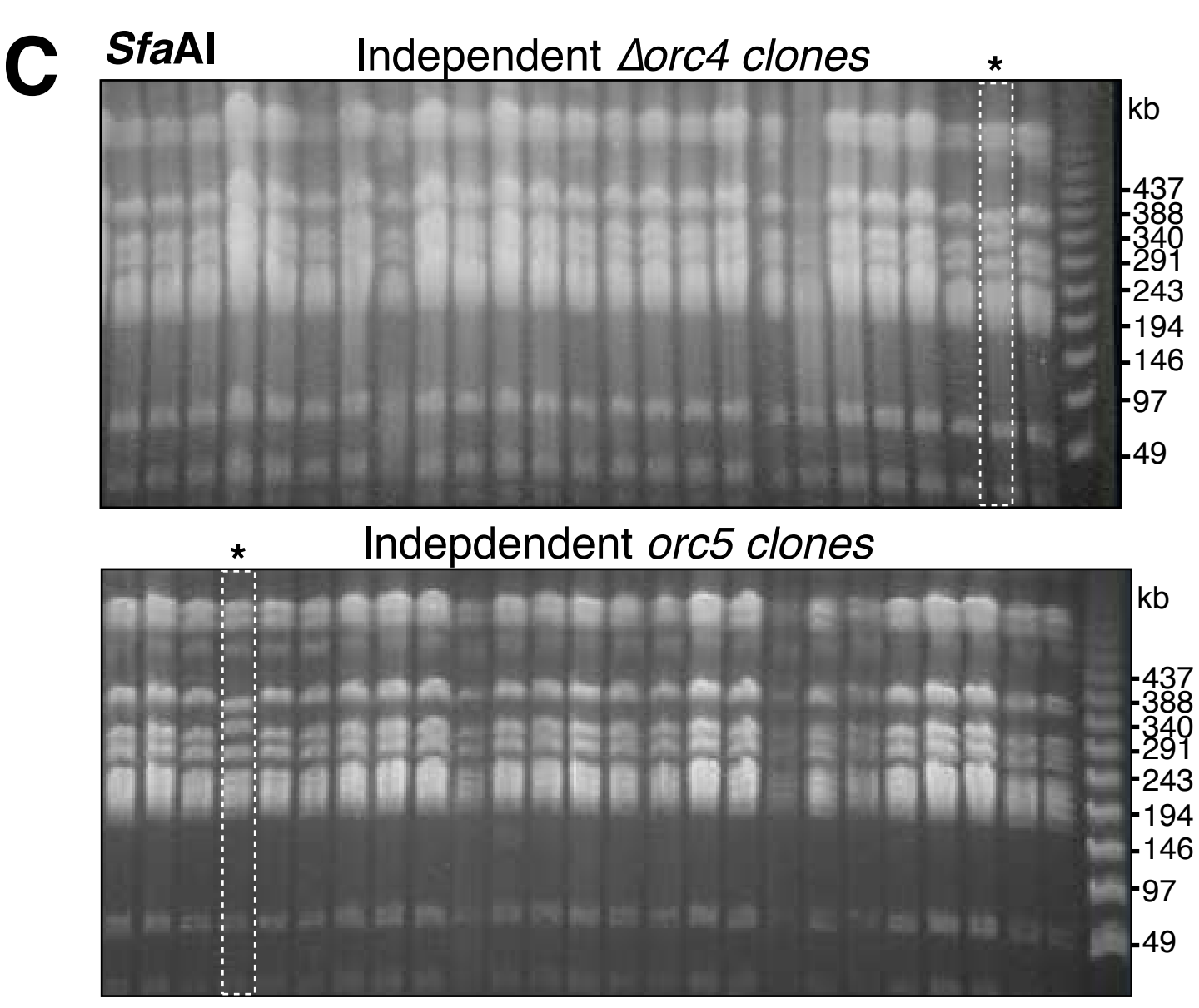

Figure 4

A

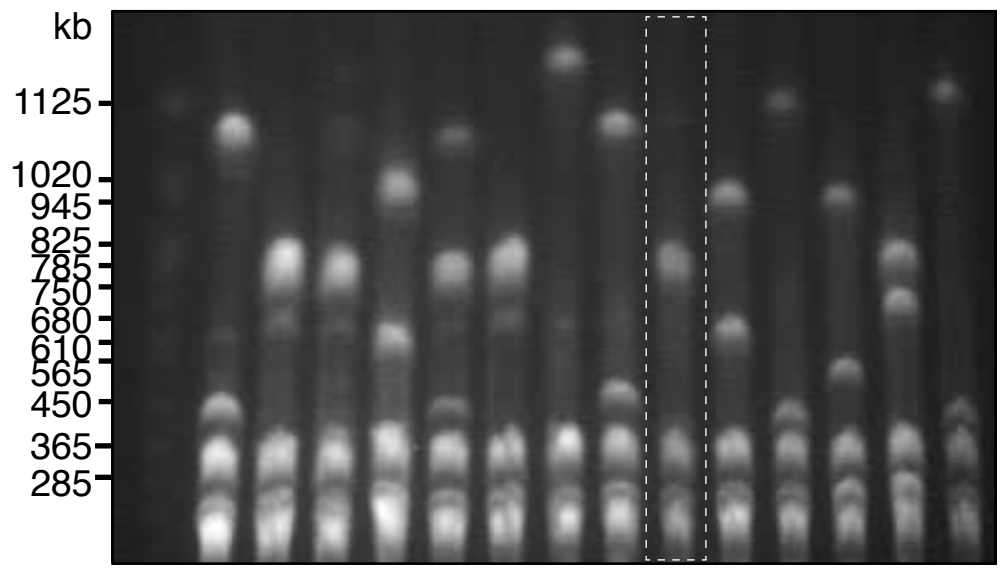

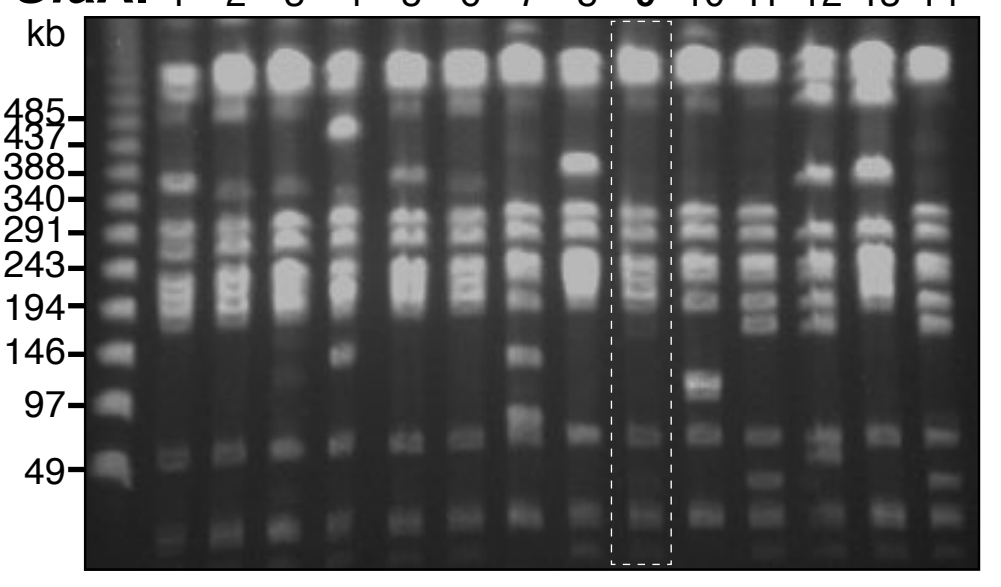

	1	2	3	4	5	6	7	8	**9**	10	11	12	13	14
Wild-type	■							■						
Polymorphic		■	■		■	■								
Monomorphic									■					
Additional rearr.				■			■			■	■	■	■	■

1. H26 WT
2. H1689 *Δorc5*
3. H1822 *Δorc5*
4. H2733 *Δorc5 Δorc3*
5. H2149 *Δorc5 Δorc9*
6. H2196 *Δorc5 Δorc1*
7. H2313 *Δorc5 Δorc2*
8. H2458 *Δorc5 Δorc3 Δorc9*
9. **H2202 *Δorc5Δorc3***
10. H2786 *Δorc5 Δorc9*
11. H2562 *Δorc5 Δorc9 Δorc2*
12. H2459 *Δorc5 Δorc1 Δorc9*
13. H3195 *Δorc5 Δp.tnaA-radA*
14. H2738 *Δorc5 Δorc3 Δorc9*

B

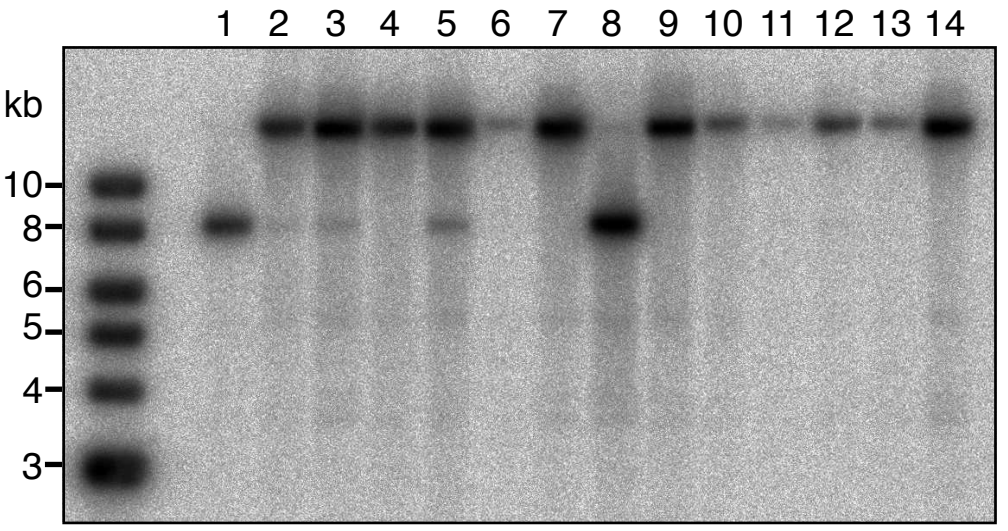

StyI cut; *sod1U* probe

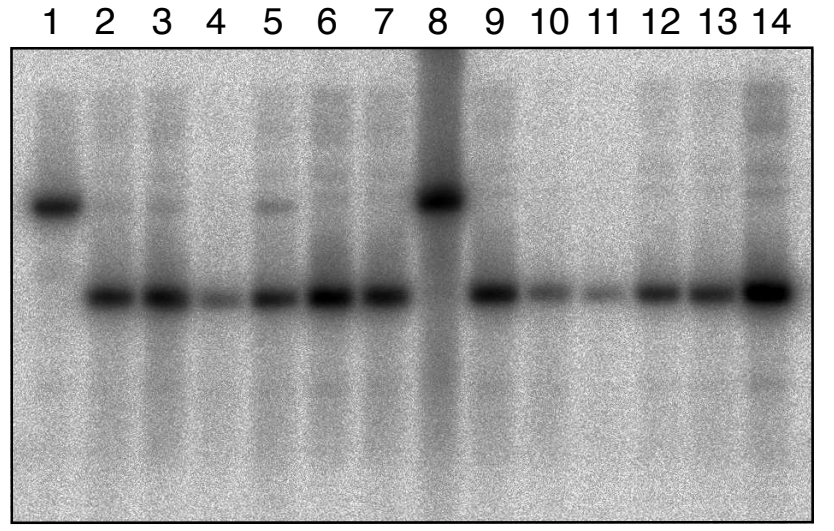

EcoRV cut; *sod2D* probe

C

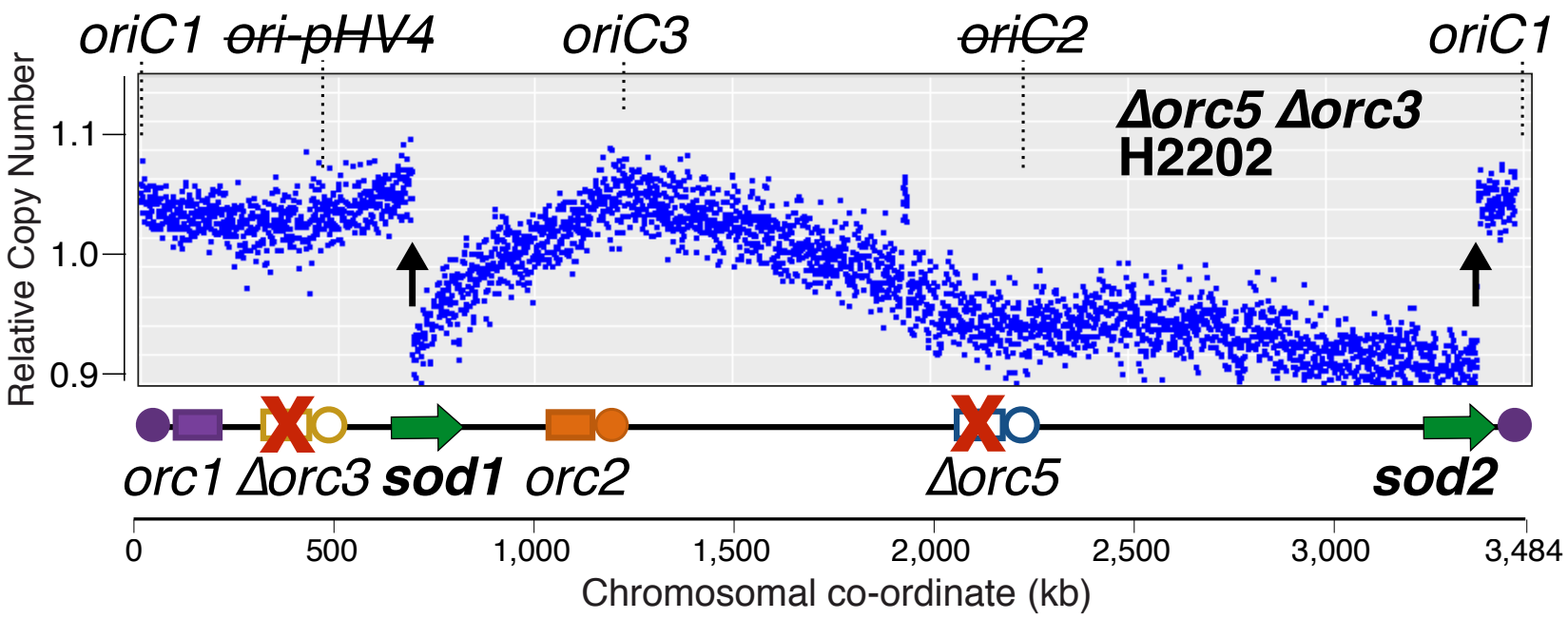

D

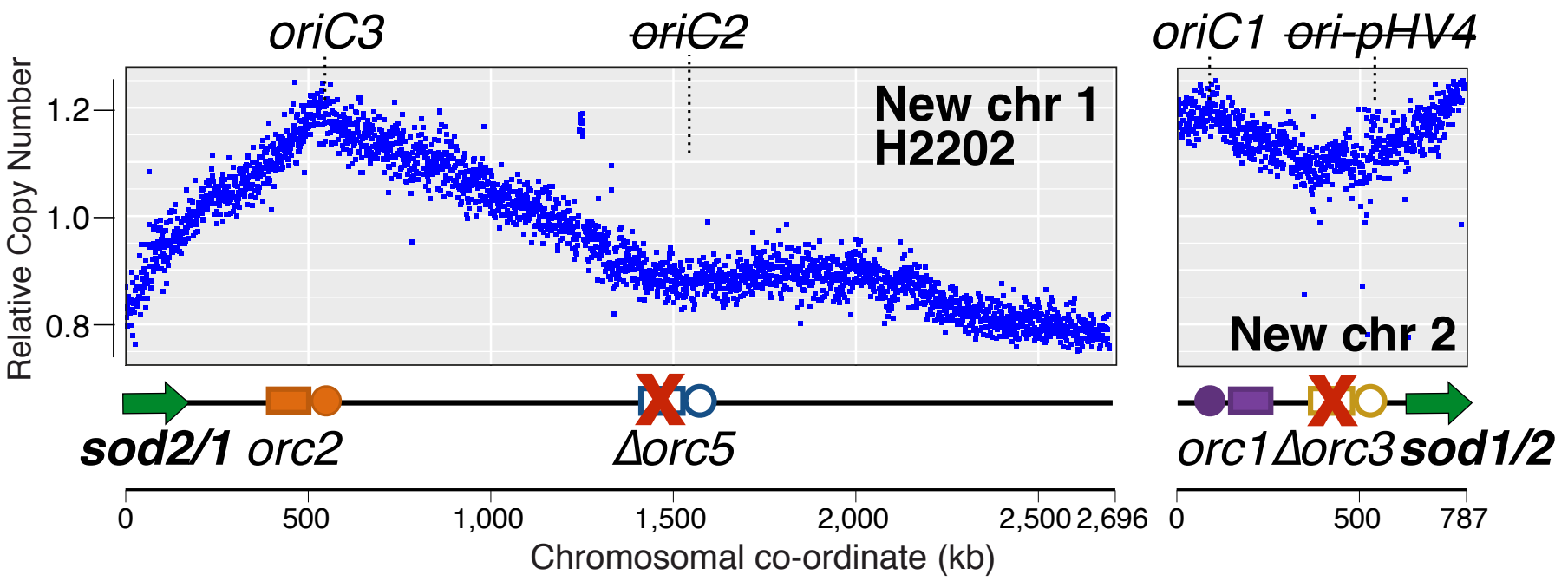

Figure 5